HHS Public Access

Author manuscript

Sci Immunol. Author manuscript; available in PMC 2023 March 11.

Published in final edited form as:

Sci Immunol. 2022 March 11; 7(69): eabm0631. doi:10.1126/sciimmunol.abm0631.

Tim-3 adapter protein Bat3 acts as an endogenous regulator of tolerogenic dendritic cell function

Ruihan Tang[1,2], **Nandini Acharya**[1,2,†,‡], **Ayshwarya Subramanian**[1,2,3], **Vinee Purohit**[1,2], **Marcin Tabaka**[3,§], **Yu Hou**[1,2], **Danyang He**[1,2,¶,#,**], **Karen O. Dixon**[1,2], **Connor Lambden**[1,2], **Junrong Xia**[1,2], **Orit Rozenblatt-Rosen**[3,††], **Raymond A. Sobel**[4], **Chao Wang**[1,2,‡‡,§§], **Aviv Regev**[3,5,††], **Ana C. Anderson**[1,2], **Vijay K. Kuchroo**[1,2,3,*]

[1]Evergrande Center for Immunologic Diseases, Harvard Medical School and Brigham and Women's Hospital, Boston, MA, USA.

[2]Ann Romney Center for Neurologic Diseases, Brigham and Women's Hospital, Harvard Medical School, Boston, MA, USA

[3]Klarman Cell Observatory, Broad Institute of MIT and Harvard, Cambridge, MA, USA.

[4]Department of Pathology, Stanford University, Stanford, CA, USA.

[5]Department of Biology, Howard Hughes Medical Institute and Koch Institute for Integrative Cancer Research, Massachusetts Institute of Technology, Cambridge, MA, USA.

Abstract

Dendritic cells (DCs) sense environmental cues and adopt either an immune-stimulatory or regulatory phenotype, thereby fine-tuning immune responses. Identifying endogenous regulators that determine DC function can thus inform the development of therapeutic strategies for modulating the immune response in different disease contexts. Tim-3 plays an important role in regulating immune responses by inhibiting the activation status and the T cell priming ability of DC in the setting of cancer. Bat3 is an adaptor protein that binds to the tail of Tim-3; therefore,

*Corresponding author. vkuchroo@rics.bwh.harvard.edu.
†Present address: Department of Neurology, Ohio State University, Wexner Medical Center, Columbus, OH, USA.
‡Present address: Pelotonia Institute for Immuno-Oncology, The Ohio State University Comprehensive Cancer Center, Columbus, OH, USA.
§Present address: International Eye Research, Institute of Physical Chemistry, Polish Academy of Sciences, Warsaw, Poland.
¶Present address: Key Laboratory of Growth Regulation and Translational Research of Zhejiang Province, School of Life Sciences, Westlake University, Hangzhou, China.
#Present address: Westlake Laboratory of Life Sciences and Biomedicine, Hangzhou, China.
**Present address: Laboratory of Systems Immunology, Institute of Basic Medical Sciences, Westlake Institute for Advanced Study, Hangzhou, China.
††Present address: Genentech, 1 DNA Way, South San Francisco, CA, USA.
‡‡Present address: Biological Sciences Platform, Sunnybrook Research Institute, Toronto, ON M4N 3M5, Canada.
§§Present address: Department of Immunology, University of Toronto, Toronto, ON M5S 1A8, Canada.

Author contributions: R.T. and V.K.K. conceived and designed the study. R.T. designed, performed, and analyzed most experiments, with significant contributions of N.A., V.P., C.W., A.C.A., and V.K.K. A.S. and M.T. performed computational analyses. R.A.S. performed histological analysis. Y.H., V.P., D.H., K.O.D., C.L., and J.X. provided further experimental/analytical assistance or provided critical materials. V.K.K., A.C.A., A.R., and C.W. supervised the study. R.T., N.A., A.C.A. and V.K.K. wrote the manuscript with contributions from all authors.

SUPPLEMENTARY MATERIALS

www.science.org/doi/10.1126/sciimmunol.abm0631

Competing interests: All other authors declare that they have no competing interests.

we studied its role in regulating the functional status of DCs. In murine models of autoimmunity (experimental autoimmune encephalomyelitis) and cancer (MC38-OVA–implanted tumor), lack of Bat3 expression in DCs alters the T cell compartment—it decreases T_H1, T_H17 and cytotoxic effector cells, increases regulatory T cells, and exhausted $CD8^+$ tumor-infiltrating lymphocytes, resulting in the attenuation of autoimmunity and acceleration of tumor growth. We found that Bat3 expression levels were differentially regulated by activating versus inhibitory stimuli in DCs, indicating a role for Bat3 in the functional calibration of DC phenotypes. Mechanistically, loss of Bat3 in DCs led to hyperactive unfolded protein response and redirected acetyl–coenzyme A to increase cell intrinsic steroidogenesis. The enhanced steroidogenesis in Bat3-deficient DC suppressed T cell response in a paracrine manner. Our findings identified Bat3 as an endogenous regulator of DC function, which has implications for DC-based immunotherapies.

INTRODUCTION

Dendritic cells (DCs) play a fundamental role in shaping the T cell landscape by controlling T cell activation, expansion, and differentiation (1). Conventional DCs (cDCs) are highly plastic cells that act as sentinels in tissue and, depending on the local milieu, can either activate T cells or induce T cell tolerance. There are two distinct cDC subsets, $CD103^+$ cDC1s and $CD11b^+$ cDC2s (2). cDC1s have a unique capacity to induce cellular immunity against intracellular pathogens and tumor cells by cross-presenting exogenous antigens to activate $CD8^+$ T cells. In contrast, cDC2s are potent inducers of $CD4^+$ T cell responses (3). Overall, in response to certain stimuli, DCs undergo maturation wherein they acquire the ability to produce higher levels of proinflammatory cytokines and chemokines and exhibit higher surface expression of costimulatory molecules and major histocompatibility complex II (MHC-II) (4). However, various physiological and pharmacological agents may induce tolerogenic DCs (tolDCs). tolDCs are not specific to a given lineage and are present in the steady state in certain anatomical sites, such as the intestine and airways, where they help maintain immune homeostasis (4). These DCs control excessive immune activation by inducing tolerance in T cells via multiple mechanisms including T cell anergy, T cell deletion, or conversion to $FoxP3^+$ regulatory T cells (T_{regs}) (4). Specifically, tolDCs often display an immature or semimature phenotype with characteristically low expression of costimulatory (e.g., CD80 and CD86) and MHC molecules on their surface, favoring weak antigen presentation, and produce anti-inflammatory cytokines, such as interleukin-10 (IL-10) and transforming growth factor–β (TGF-β), facilitating an anti-inflammatory microenvironment (4). Thus, the functional status of DCs is essential for the maintenance of immunological homeostasis.

The unique capacity of DCs to induce both immune activation and tolerance has been exploited for the development of several immunotherapeutic strategies for patients with autoimmune diseases such as rheumatoid arthritis (5), type 1 diabetes (6), and multiple cancers (7). However, the therapeutic potential of DC-directed therapies remains to be fully exploited in the clinic because DCs change their function in vivo due to high plasticity, resulting in short-lived effects (8, 9). Accordingly, the development of reliable and effective DC-directed therapies requires identification of endogenous regulators that can be genetically modified to modulate DC function to achieve the desired stable effects. Such

endogenous regulators that can switch DCs between the regulatory and stimulatory states are under studied.

Tim-3 regulates DC function by inhibiting the activation of the inflammasome (10) and inhibiting the stimulator of interferon genes (STING) pathway in DCs (11). Because Bat3 is an adapter protein that binds to the cytoplasmic tail of Tim-3 and restrains its inhibitory function (12), therefore, it was tempting to hypothesize that Bat3 may function as an endogenous regulator of DCs function. Bat3 is encoded by *Bag6*, which is located within the MHC class III gene cluster on chromosome 6; the latter encodes genes with key roles in immune function (13, 14). Bat3 polymorphisms are associated with an increased incidence of several autoimmune diseases such as Kawasaki syndrome (15), type 1 diabetes (16), rheumatoid arthritis (17), and allogeneic hematopoietic stem cell transplant (18), as well as lung cancer (19, 20), indicating that Bat3 may be involved in the regulation of wide spectrum of immune-mediated diseases.

Here, we examined the effect of selective loss of Bat3 on regulating the functional activity of DCs. We found that Bat3 expression was tightly regulated by stimulatory versus regulatory signals, with Bat3 being higher in immune stimulatory compared with tolDCs. Conditional deletion of Bat3 in DCs drove the acquisition of regulatory-like phenotype, thereby inhibiting both autoimmunity and antitumor immunity. Mechanistically, loss of Bat3 altered endoplasmic reticulum (ER) homeostasis and rewired cellular metabolism to increase the production of steroid hormones by inhibiting the tricarboxylic acid cycle (TCA cycle). $Bat3^{-/-}$ DCs showed increased production of glucocorticoid, which acted on T cells in a paracrine manner to suppress immune responses. Our findings suggest that Bat3 is an endogenous regulator of the tolerogenic state in DCs with important implications for regulating autoimmunity and antitumor immunity.

RESULTS

The absence of Bat3 expression in DCs alters the cross-talk between DCs and T cells

To study the cell-intrinsic function of Bat3 in regulating DC functions, we used $Bat3^{fl/fl}CD11c^{CRE}$ [hereby referred to as Bat3 conditional knockout (cKO)] mice (21). First, we confirmed that Bat3 was selectively deleted in $CD11c^{+}$ DCs (fig. S1, A and B). Next, we determined that the absence of Bat3 in $CD11c^{+}$ cells did not affect the proportion nor the number of major immune populations [DCs, T cells, B cells, natural killer (NK) cells, and NKT cells] (fig. S1, C to E) and confirmed that Bat3 was dispensable for the development and survival of DCs at steady state.

The functional status of DCs can determine whether immune activation versus tolerance ensures. We therefore investigated the effect of Bat3 modulation in DC in a model of autoimmunity. To study the effect of loss of Bat3 in DCs in autoimmunity, we induced experimental autoimmune encephalomyelitis (EAE) in Bat3 cKO mice and their littermate controls by immunization with $MOG_{35–55}$ (myelin oligodendrocyte glycoprotein 35–55) peptide. We observed that the Bat3 cKO mice developed significantly milder clinical disease compared with the controls (Fig. 1A). Histopathologic analysis confirmed that Bat3 cKO mice had less severe inflammation compared with controls (Fig. 1B). We assessed the

central nervous system (CNS) infiltrates and found that changes in the frequency and total cell numbers of plasmacytoid DC, myeloid DCs, and cDCs were not significant (fig. S2, A to C). Neither the proportion of Tim-3$^+$ CNS-infiltrating cDCs nor their expression level of Tim-3 was different between the Bat3 cKO mice and controls (fig. S2D). Furthermore, we observed that there was no difference in the frequency of cDC1 and cDC2 subsets in the CNS of Bat3 cKO and the controls (fig. S2E). However, although we did not observe differences in the abundance of DCs (fig. S2, B and C) or distribution of DC subsets (fig. S2E), examination of their phenotype revealed that in the absence of Bat3, DCs had lower expression of MHC-II, CD40, CD80, CD86, and programmed cell death ligand 1 (PDL1) (Fig. 1D and fig. S2, C and F). The absence of Bat3 expression on DCs also affected CD4$^+$ T cells in the CNS. Specifically, we found that the Bat3 cKO mice harbored fewer total and proinflammatory IL-17A$^+$ and interferon-γ–positive (IFN-γ$^+$) CD4$^+$ T cells (fig. S2G) but more FoxP3$^+$ CD4$^+$ T cells (T_{regs}) in the CNS compared with controls at the peak of disease (Fig. 1D and fig. S2G). We next included 5-bromo-2′-deoxyuridine (BrdU) staining to assess the proliferation status of T_{regs}, T helper 17 (T_H17) cells, and T_H1 cells retrieved from the draining lymph nodes (dLNs) and CNS of the Bat3 cKO mice and the controls at the peak of disease. The Bat3 cKO mice exhibited a significant reduction in the proliferation of IL-17A$^+$ and IFN-γ$^+$ T cells but an increase in the proliferation of T_{regs} in both the dLN and CNS (fig. S2H). These data indicated that the absence of Bat3 expression in DCs led to the establishment of a phenotype that shared many features with regulatory DCs, including the ability to suppress proinflammatory T cell responses.

Autoimmunity and cancer are at opposite ends of the spectrum of immune activation. Having observed that the loss of Bat3 in DCs ameliorated CNS autoimmunity, we next investigated whether it would weaken antitumor immunity. We found that Bat3 cKO mice exhibited faster tumor growth compared with controls in the MC38-OVA^{dim} model of colon carcinoma (Fig. 1E). To examine how the loss of Bat3 in DCs affected the function of DCs and potentially DC–T cell cross-talk in the tumor microenvironment (TME), we harvested tumors at an early stage of tumor development when tumor sizes (40 to 60 mm^2) were not significantly different across the two groups of mice (22). Consistent with our observations in the DCs from the CNS of mice undergoing EAE, we found no significant differences in either the absolute numbers or the frequency of total cDC and DC subsets in the tumor tissues of the Bat3 cKO and control mice (fig. S3, A to D); however, the DCs from the TME in Bat3 cKO mice also exhibited lower levels of CD40, CD86, CD80, and PDL1 (Fig. 1F and fig. S3E) compared with their controls. In addition, there were fewer CD8$^+$ tumor-infiltrating lymphocytes (TILs) in the TME of Bat3 cKO mice (fig. S3F). We next examined the phenotype of the CD8$^+$ TILs in the Bat3 cKO mice. Tim-3 and programmed cell death 1 (PD1) can be used to identify terminally exhausted CD8$^+$ TILs (23). Therefore, we compared the frequency of Tim-3$^+$PD1$^+$CD8$^+$ TILs between the Bat3 cKO and the controls; we observed a higher frequency of Tim-3$^+$PD1$^+$CD8$^+$ TILs in Bat3 cKO mice (Fig. 1G). CD8$^+$ TILs from Bat3 cKO mice also exhibited lower cytotoxic capacity, as shown by the decreased frequency of CD107a$^+$Granzyme B$^+$ cells. The CD8$^+$ TILs from Bat3 cKO mice exhibited dampened responses to ex vivo polyclonal restimulation, producing less IL-2, tumor necrosis factor–α (TNF-α), and IFN-γ and were less polyfunctional (Fig. 1G and fig. S3G). Together, these findings demonstrated that Bat3 expression in DCs directly affected

their functional status, leading to the modulation of $CD4^+$ and $CD8^+$ T cells in autoimmune and tumor settings.

Bat3 regulates the functional plasticity of DCs in vivo

To gain a better understanding of the role of Bat3 in DCs in regulating T cell function in vivo, we studied the expansion and differentiation of MOG-specific T cell receptor (TCR) ($V\alpha 3.2^+$) bearing T cells (24) referred to as 2D2 cells upon transfer into either Bat3 cKO or littermate controls immunized with $MOG_{35–55}$ peptide (Fig. 2A). After immunization, we examined the proliferation status of the 2D2 cells and found that there was a reduction in their proliferation in the dLNs and CNS of Bat3 cKO mice (Fig. 2B). Moreover, 2D2 cells retrieved from the Bat3 cKO mice exhibited a significant reduction in IL-$17A^+$ and IFN-γ^+ but an increase in IL-10^+ T cells (Fig. 2C). Together with the data in Fig. 1D, these findings reinforced the notion that the absence of Bat3 in DCs dampened the expansion of effector T cells and the production of proinflammatory cytokines in the establishment of autoimmunity. Furthermore, DCs derived from Bat3 cKO mice supported the antigen-specific differentiation of $FoxP3^+$ T cell (T_{regs}) from 2D2 cells in the dLN and CNS (Fig. 2D).

We next tested whether DCs deficient in Bat3 acquired the ability to actively induce tolerance in vivo. We pulsed bone marrow–derived DCs (BMDCs) generated from Bat3 cKO mice or controls with $MOG_{35–55}$ peptide and transferred these antigen-pulsed DCs to wild-type (WT) recipient mice that were previously immunized with $MOG_{35–55}$ (Fig. 2E). We found that MOG-pulsed Bat3-deficient DCs ($Bat3^{-/-}$ DCs) significantly inhibited the development of actively induced EAE with reduction in both clinical disease and lesion load (Fig. 2F). Together, these data demonstrated that the absence of Bat3 in DCs led to acquisition of tolerogenic features by DCs.

Next, we studied in detail the phenotype of the DCs derived from the Bat3 cKO mice in vitro. In line with our data in the EAE and colorectal tumor models (Fig. 1), we found that after lipopolysaccharide (LPS) stimulation, the $Bat3^{-/-}$ DCs had lower frequencies of MHC-II^+, $CD40^+$, $CD80^+$, $CD86^+$, $PDL1^+$, and $PDL2^+$ cells (Fig. 2G). In the steady state, $Bat3^{-/-}$ DCs also had a significantly lower frequency of $CD80^+$ but a higher frequency of $PDL2^+$ cells (fig. S4A). To determine how the changes observed in the DC phenotype affected DC–T cell cross-talk, we performed DC–T cell coculture assays. To this end, we used an in vitro system where DCs pulsed with $MOG_{35–55}$ peptide were cocultured with MOG-specific (2D2) naïve T cells. The priming ability of DCs was assessed by comparing T cell proliferation and cytokine production after coculture. Consistent with their markedly diminished maturation status, $Bat3^{-/-}$ DCs showed reduced ability to prime naïve 2D2 T cells, resulting in a much lower rate of T cell proliferation (Fig. 2H). Again, reminiscent of our data from the CNS of Bat3 cKO during EAE (Figs. 1, A to D, and 2, A to D), we found that $Bat3^{-/-}$ BMDCs also had an impaired ability to polarize naïve T cells toward IFN-γ^+ and IL-$17A^+$ T cells but rather promoted an increase in the frequency of IL-10^+ and $FoxP3^+$ T cells (Fig. 2I).

We next tested whether the absence of Bat3 expression in DCs affected their antigen processing ability. Full-length MOG protein is relatively unstable; thus, we used the

ovalbumin (OVA) protein and peptide system. We pulsed the Bat3-sufficient ($Bat3^{+/+}$) and $Bat3^{-/-}$ DCs with OVA protein or OVA peptide (ISQAVHAAHAEINEAGR or SIINFEKL), followed by coculturing these cells with OVA-specific $CD4^+$ T cells (OT-II or OT-I). We found that $Bat3^{-/-}$ DCs demonstrated reduced capacity to induce the proliferation of T cells when pulsed with either OVA protein or OVA peptide (fig. S4, B and C), indicating that the absence of Bat3 limited the ability of the DCs to process and present antigens to T cells. To further support the concept, tumor-associated DCs (tDCs) (DC1 and DC2 separately) were sorted from the Bat3 cKO mice and controls, pulsed with full-length OVA, and cocultured with either OT-I or OT-II naïve T cells, respectively. We found that $Bat3^{-/-}$ tDCs had decreased capacity to induce OT-I and OT-II T cell expansion compared with WT tDCs (Fig. 2J). Common features of tolDCs include low antigen presentation capacity combined with the loss or reduction of costimulatory signals, expression of inhibitory molecules, and an anti-inflammatory cytokine profile (4). Thus, our data suggest that loss of Bat3 promoted the acquisition of regulatory functions in DCs, leading to the suppression of T cell responses.

The expression level of Bat3 is regulated by microenvironmental cues

In response to Toll-like receptor (TLR) agonists (i.e., LPS and CpG-containing DNA) or proinflammatory cytokines (i.e., IFN-γ), DCs undergo functional maturation and activation, which subsequently leads to efficient T cell priming (25). In contrast, treatment with anti-inflammatory agents such as dexamethasone (DEX) (26, 27), vitamin D3 (28), IL-10 (29), vasoactive intestinal peptide (30), retinoic acid (31), rapamycin (32), aspirin (33), cyclosporin A (34, 35), and hepatocyte growth factor (36) leads to tolDCs with regulatory features. To dissect the association between Bat3 expression and the immune-stimulatory versus regulatory status of DCs, we treated DCs with either proinflammatory stimuli such as various TLR ligands or anti-inflammatory agents such as DEX and then examined the expression level of Bat3. We found that the proportion of $Bat3^+$ cells and the Bat3 expression levels were significantly up-regulated under the immune-stimulatory conditions (Fig. 3A and fig. S5A) and were down-regulated under the regulatory conditions at both the protein (Fig. 3A and fig. S5, A and B) and transcript (fig. S5C) levels. These data indicated that Bat3 expression was correlated with the external cues received by the DCs.

Next, we addressed whether Bat3 expression was affected by the microenvironment associated with different disease settings. To this end, we analyzed the level of Bat3 in DCs isolated from inflammatory settings (MOG-immunized EAE mice) or an immune-suppressive environment ($MC38\text{-}OVA^{dim}$ tumor-bearing mice) (Fig. 3B). Analysis of DCs from the spleen and dLN revealed an expression pattern of Bat3 consistent with that observed in vitro in BMDCs with different activation statuses; the proportion of $Bat3^+$ cells was higher in the setting of EAE, whereas it was markedly decreased in the context of tumor-bearing mice compared with that in naïve mice. The frequency of $Bat3^+$ DCs infiltrating the CNS during EAE was significantly higher than that in tumor tissue (Fig. 3B). Thus, Bat3 was induced in DCs upon proinflammatory cues both in vitro and in vivo.

The CNS T cell landscape is altered in the absence of Bat3 expression in DCs

To elucidate the impact of Bat3 expression in DCs on shaping the T cell landscape during neuroinflammation, we performed single-cell RNA sequencing (scRNA-seq) of CNS-

infiltrating T cells at the onset of EAE in WT or Bat3 cKO mice. After dimensionality reduction and graph-based clustering, we identified 13 lymphocyte subsets, including four $CD8^+$ subsets and six $CD4^+$ subsets, each with unique signature genes (Fig. 4, A to D). Cluster 3 ($CD4^+$ naïve-like T cells), cluster 11 ($CD8^+$ naïve-like T cells), and cluster 12 ($CD8^+$ NKT cells) were the main populations of T cells derived from the Bat3 cKO mice (Fig. 4B). Both the major $CD4^+$ T (cluster 3) and $CD8^+$ T cell clusters (cluster 11) in Bat3 cKO mice *Tsc22d3* emerge as an identity gene, being among the top 5 differentially expressed (DE) marker genes (Fig. 4C) along with *Rpl35*, *Lef1*, *Ccr7*, *Igfbp4*, *Rps27*, and *Rps29*. Next, we examined the DE genes between T cells derived from control and Bat3 cKO mice within each cluster. *Tsc22d3* again emerged among the top DE genes across most T cell clusters (except $CD4^+$ memory-like, T_H17-like, T_H1-like, and $CD8^+$ T stem cell–like early effector clusters) with positive expression log fold changes in the cells from the Bat3 cKO mice (Fig. 4D). Thus, *Tsc22d3* was associated with the phenotypes of T cells from the Bat3 cKO mice both at the cell subset–specific (cluster 3 and cluster 11) and pan T cell level. *Tsc22d3* encodes for glucocorticoid-induced leucine zipper (GILZ) (37). GILZ is a protein with multiple biological roles that is up-regulated by glucocorticoids, which have potent immunosuppressive functions (37). One of the mechanisms by which glucocorticoids induce immunosuppression is through regulation of the T cell response (37). Other notable genes associated with the T cells that derived from the Bat3 cKO mice were *Zfp36l2* and *Pik3ip1*, both known glucocorticoid receptor (GR) target genes (38–43). *Pik3ip1* is also a T cell regulator that leads to reduced antitumor immunity (40, 41). These data indicated that glucocorticoid signaling is more active in the T cells derived from the Bat3 cKO mice. We confirmed that the other top DE genes (*Lef1* and *Igfbp4*) were glucocorticoid responsive in T cells by examining the expression of these genes in in vitro–differentiated $CD4^+$ or $CD8^+$ T cells treated with glucocorticoids (fig. S6A). We further examined the levels of other known glucocorticoid-responsive genes such as *Mt1*, *Mt2*, *Nfil3*, *Havcr2*, and *Pdcd1* and found that these genes were also higher in the T cells retrieved from the dLN of Bat3 cKO mice with EAE compared with controls, supporting the notion that these cells indeed have a higher level of glucocorticoid signaling (Fig. 4E). This finding prompted us to hypothesize that the T cells from the CNS of Bat3 cKO mice were either more sensitive to glucocorticoids or exposed to a higher concentration of glucocorticoids in the local tissue microenvironment. We tested the first possibility by measuring the level of *Nr3c1* (gene that encodes the GR) in T cells. We found that the levels of *Nr3c1* were comparable in the $CD4^+$ T cells derived from the control or Bat3 cKO–immunized mice (fig. S6B). This finding supported the alternate hypothesis that the T cells from Bat3 cKO mice were in an environment with higher glucocorticoid content.

We therefore tested whether higher glucocorticoid production in the tissue microenvironment was the major driver of the regulatory phenotype observed in mice that lack Bat3 in DCs. We used an in vitro DC–T cell coculture system with WT or $Bat3^{-/-}$ BMDCs cocultured with either WT or GR-deficient $CD4^+$ T cells ($Nr3c1^{fl/fl}$ $dLck^{CRE}$; GR cKO) (fig. S6C) (22). In line with our previous observations (Fig. 2H), we found that $Bat3^{-/-}$ BMDCs exhibited poor stimulatory capacity when cocultured with WT T cells; however, the inhibitory effect of $Bat3^{-/-}$ BMDCs was abrogated when they were used to stimulate T cells that lack the expression of GR (Fig. 4F and G). These results indicated

that the difference in the stimulatory capacity of Bat3$^{+/+}$ versus Bat3$^{-/-}$ DCs was dependent on the presence of active glucocorticoid signaling in T cells. Similarly, we found that the differential ability of the Bat3-deficient versus Bat3-sufficient DCs to polarize T cells toward IFN-γ^{+} and IL-17A^{+} cells was completely abrogated when using GR-deficient T cells (Fig. 4G). We further tested the requirement for active glucocorticoid signaling in T cells in vivo. We transferred Bat3$^{-/-}$ BMDCs to either WT or GR cKO mice. As expected, the transfer of Bat3$^{-/-}$ BMDCs resulted in inhibition of EAE in WT mice. Conversely, the transfer of Bat3$^{-/-}$ DCs to GR cKO recipients abolished the previously observed regulatory effect of Bat3$^{-/-}$ DCs (Fig. 4H). Together, these data indicated that the regulatory effect of Bat3$^{-/-}$ DCs on CD4^{+} T cells was largely dependent on the activation of glucocorticoid signaling in the interacting T cells.

Enhanced activation of the unfolded protein response leads to acquisition of regulatory-like features in Bat3-deficient DCs

Our data pointed to a role for glucocorticoids in the regulatory phenotype of Bat3$^{-/-}$ DCs. Myeloid cells are a major local source of endogenous glucocorticoids in the TME (22). Accordingly, we tested the steroidogenic capacity of DCs by examining the expression of the enzymes involved in glucocorticoid biosynthesis (*StAR*, *Cyp21a1*, *Cyp11b1*, *Hsd3b3*, and *Hsd11b1*) in the Bat3$^{+/+}$ versus Bat3$^{-/-}$ DCs. All these genes were expressed at a higher level in dLN DCs derived from $MOG_{35–55}$ peptide–immunized Bat3 cKO (Fig. 5A). We further confirmed that Bat3$^{-/-}$ DCs produce significantly higher amounts of corticosterone as compared with Bat3$^{+/+}$ DCs (Fig. 5B).

As the absence of Bat3 led to the acquisition of regulatory-like features by the DCs (Figs. 1 and 2), we assessed whether the transcriptome of Bat3$^{-/-}$ DCs shared features with those of other bona fide tolDCs generated by treatment with IL-10/TGF-β, rapamycin, or vitamin D3. We found that regulatory DCs generated by these treatments shared some features with Bat3-deficient DCs (e.g., TNF signaling, phagosome, and osteoclast differentiation); however, Bat3$^{-/-}$ DCs mostly adopted unique programs that correlated with their regulatory functions (fig. S7, A to C). To further dissect the unique mechanisms by which Bat3 regulated DC functions, we focused on the differences in the transcriptional profiles between the Bat3-deficient and Bat3-sufficient DCs (Fig. 5C and fig. S7D). We noted that Bat3$^{-/-}$ DCs had markedly increased the expression of *Ern1*, *Atf4*, and *Ddit3*, genes involved in hyperactivation of the unfolded protein response (UPR) (Fig. 5C). We further confirmed that Bat3$^{-/-}$ DCs had marked up-regulation of additional ER stress–related genes, including *Xbp1s*, *Sec61a1*, *Erdj4*, *Gadd34*, *Grp94*, and *Grp78* (Fig. 5D). Accordingly, “response to unfolded protein” (GO:0006986) or “protein processing in the endoplasmic reticulum” (mmu04141) (fig. S6C) were among the top-ranked pathways [false discovery rate (FDR) < 0.05] enriched in the Bat3$^{-/-}$ DCs. These pathways supported the idea that Bat3 is a chaperone protein that acts as a hub in protein quality control pathways to prevent aggregation and accumulation of misfolded and mislocalized protein (44–49). Bat3$^{-/-}$ BMDCs showed increased splicing of *Xbp1* mRNA and higher spliced form of X-box binding protein 1 (XBP1s) nuclear levels compared with WT controls (fig. S7, E and F). Together, these data indicated that Bat3 may regulate DC function by controlling the level of the UPR.

Given that sustained hyperactivation of the UPR is a unique feature of Bat3$^{-/-}$ DCs, we next examined whether this feature imparted regulatory properties to the DCs. We first tested whether normalizing or relieving the ER stress in Bat3$^{-/-}$ DCs could revert the regulatory status of Bat3$^{-/-}$ DCs in vitro. For this, we used two highly potent and specific ER stress inhibitors [4-phenylbutyric acid (4PBA) and 7-hydroxy-4-methyl-2-oxo-2H-1-benzopyran-8- carboxaldehyde (4μ8C)]. 4PBA mainly targets the inositol-requiring enzyme 1α (IRE1α)/XBP1 axis in addition to two other UPR pathways (50), and 4μ8C is a selective inhibitor of IRE1-dependent degradation and splicing of *Xbp1* mRNA in response to ER stress (51). Treatment with 4PBA or 4μ8C of in vitro LPS-stimulated BMDCs rescued the defective activation of Bat3$^{-/-}$ DCs as shown by increased expression of MHC-II, CD40, CD80, CD86, PDL1, and PDL2 (Fig. 5E and fig. S8A) and resulted in a dose-dependent restoration of the proliferative response of T cells upon coculture (Fig. 5F and fig. S7B). We next confirmed the effect of targeting the UPR in Bat3$^{-/-}$ DCs in vivo. We transferred Bat3$^{-/-}$ DCs treated with 4PBA or 4μ8C to MOG-immunized mice and found that mice receiving 4PBA- or 4μ8C-treated DCs enhanced the severity of EAE (Fig. 5G), correlating to increased infiltration of CD4^{+} T cells expressing higher levels of IFN-γ and IL-17 into the CNS but reduced frequency of FoxP3^{+} T_{regs} (Fig. 5H). Similarly, we found that adoptive transfer of Bat3$^{-/-}$ DCs pretreated with 4PBA to MC38-OVA^{dim} tumor-bearing mice completely abolished the previously observed tumor-promoting effects of these DCs (Fig. 5I), reduced the proportions of Tim-3^{+}PD1^{+} CD8 TILs, and increased the production of IFN-γ and TNF-α by CD8^{+} TILs, indicating that the restriction of ER stress in Bat3$^{-/-}$ DCs reduced their regulatory phenotype and improved their ability to mount effective antitumor responses (Fig. 5J). Further, intratumoral administration of 4PBA at an early stage of tumor progression (average tumor size < 40 mm^2), when tumor sizes were not significantly different across groups, abrogated the accelerated tumor progression observed in the Bat3 cKO mice (fig. S8C), reduced the frequency of PD1^{+}Tim-3^{+}CD8^{+} TILs, and increased the production of IFN-γ and TNF-α by CD8^{+} TILs (Fig. S8D). Collectively, these data indicated that targeting the ER stress response in Bat3$^{-/-}$ DCs reduced the tolerogenicity of these cells, which subsequently led to augmented T cell activation.

Bat3-mediated ER stress regulation controls cell-intrinsic steroidogenesis in DCs

We next examined a connection between ER stress and the induction of steroidogenesis in DCs. We noted that enzymes in the TCA cycle (*Aco1*, *Idh1*, *Idh3a*, *Sdha*, and *Sdhb*) were significantly down-regulated in the Bat3$^{-/-}$ compared with Bat3$^{+/+}$ DC (Fig. 5C). Aconitase (Aco1) and isocitrate dehydrogenase (Idh) mediate conversion of mitochondrial citrate to isocitrate and α-ketoglutarate, respectively, and their inhibition redirects citrate to cytoplasmic lipid and sterol synthesis (52). We hypothesized that ER stress and activation of the UPR redirect central carbon metabolism from the TCA cycle toward steroidogenesis by reduced expression of TCA cycle enzymes. Lack of Bat3 reduced expression of multiple genes in the TCA cycle of in vitro LPS-stimulated BMDCs, and these were rescued by treatment with 4PBA (Fig. 6A). This was concomitant to an increased expression of *Acly* and levels of acetyl–coenzyme A (acetyl-CoA), both of which indicated an increased synthesis of cytoplasmic acetyl-CoA in the Bat3$^{-/-}$ compared with Bat3$^{+/+}$ BMDCs (Fig. 6A and B). Acetyl-CoA is resynthesized in the cytoplasm from citrate exported from mitochondria and is required for lipid synthesis (53). In agreement with the elevated levels

of acetyl-CoA in the Bat3$^{-/-}$ DCs, the levels of citrate were also higher compared with the WT controls (Fig. 6B). Simultaneously, there was reduced flux of citrate in TCA cycle as measured by the level of the TCA cycle intermediate fumarate, which was significantly reduced in Bat3$^{-/-}$ DCs (Fig. 6B).

Our data pointed to increased lipid and sterol synthesis in Bat3$^{-/-}$ DCs. We found that Bat3$^{-/-}$ DCs had significantly increased cholesterol and that this was completely abrogated by treatment with 4PBA (Fig. 6B). Because cholesterol is a metabolic intermediate bridging acetyl-CoA and steroids, we determined whether inhibiting ER stress reversed not only changes in the levels of the above intermediates but also the increase in steroid levels (Fig. 6B). Restraining the UPR by treatment with ER stress inhibitors [4PBA, 4μ8C, B-I09 (54), and MKC8866 (55)] or by genetic ablation of Xbp1 [Xbp1$^{fl/fl}$CD11c^{CRE} mice (56)] reduced the level of corticosterone in Bat3$^{-/-}$ DCs to the same level measured in WT counterparts (Fig. 6C and fig. S8E). To further test this in vivo, we examined the expression of the enzymes involved in glucocorticoid biosynthesis (*StAR*, *Cyp21a1*, *Cyp11b1*, *Hsd3b3*, and *Hsd11b1*) in the dLN DCs derived from MOG immunized Bat3fl/fl, Bat3fl/flCD11cCRE, and Xbp1fl/flBat3fl/flCD11cCRE mice. Conditional deletion of Xbp1 in Bat3$^{-/-}$ DCs (fig. S6D) reduced the expression level of these enzymes to the levels observed in controls (Fig. 6D). In addition, genetic ablation of Xbp1 in Bat3$^{-/-}$ DCs reduced the level of glucocorticoid-responsive genes in responding CD4^{+} and CD8^{+} T cells in the dLNs of the double KO mice (Fig. 6E). Hence, our findings indicated that Bat3 is a regulator of the fate of the acetyl-CoA pool in BMDCs. Genetic ablation of Bat3 in DCs promoted ER stress that inhibited central carbon metabolism in the TCA cycle and directed acetyl-CoA toward steroidogenesis.

In the current study, we showed that (i) the absence of Bat3 expression in DCs ameliorates autoimmunity but enhances tumor growth; (ii) the absence of Bat3 in DCs leads to the development of a tolDC phenotype that affects DC–T cell cross-talk; (iii) the expression level of Bat3 in DCs is markedly increased by proinflammatory stimuli but decreased by anti-inflammatory stimuli; (iv) DCs deficient in Bat3 develop unresolved ER stress, which redirects acetyl-CoA toward enhanced steroidogenesis; and (v) glucocorticoids produced by Bat3-deficient DCs induce T cell tolerance both in vitro and in vivo. Together, these results indicated that Bat3 had a central role in limiting the UPR response. Loss of Bat3 activated ER stress, which, in turn, inhibits the TCA cycle, leading to the accumulation of citrate, which served as a substrate for synthesis of cholesterol that is broken down to produce glucocorticoids. DC-derived glucocorticoids acted on T cells to inhibit autoreactive T cell responses in EAE and antitumor T cell responses in MC38 colon carcinoma (Fig. 7).

DISCUSSION

DCs are sentinel cells that integrate signals from the environment and either pave the way for the induction of immunity or set up a state of tolerance. Although various external stimuli that can skew the functional state of DCs have been identified (57, 58), the endogenous molecular switches that can regulate the functional state of DCs remain elusive. Here, we described that Bat3 can act as an endogenous regulator of the functional state of DCs. Our data demonstrate a previously unknown Bat3-regulated metabolic mechanism

of determining the immunogenic versus tolerogenic state in DCs. Hence, Bat3$^{-/-}$ DCs show reduced expression of TCA cycle genes (*Aco1*, *Idh1*, *Idh3a*, *Sdha*, *Sdhb*, *Suclg1*, and *Dlat*) and reduction of TCA cycle metabolites, which reverses upon inhibition of UPR. This is concurrent with increased acetyl-CoA, citrate, and cholesterol levels in Bat3$^{-/-}$ DCs, all being precursors of steroids including glucocorticoids. TCA cycle regulates ER stress in hepatocytes by increased glutathione oxidation (59). Although these findings remain to be investigated in DCs, our study showed that ER stress could also reduce TCA cycle metabolism to promote steroid biosynthesis. This indicates a potential positive feedback loop between ER stress and TCA cycle metabolites. Accumulation of cholesterol, a precursor to glucocorticoids, increases DC activity, although this is contingent upon inhibition of Abca1/g1 transporters (60). Bat3 deficiency increased expression of these transporters based on our quantitative polymerase chain reaction (qPCR) results. Our data showed glucocorticoid-promoted regulatory phenotypes in T cell. Likewise, exogenous cholesterol promotes FoxP3^{+} T_{regs} under hypercholesterolemia (61). Hence, Bat3$^{-/-}$ DC could be releasing both cholesterol and glucocorticoid to promote T_{reg} phenotypes in a tumor or autoimmune environment. Further studies are warranted to determine whether this effect is additive or only through glucocorticoid.

Glucocorticoids are routinely used to generate tolDCs in vitro and in clinical settings (62, 63). Glucocorticoid can also be produced by myeloid cells in the TME (22). Here, we demonstrate that the regulatory effect of Bat3$^{-/-}$ DCs was dependent on the activation of glucocorticoid signaling in the interacting T cells. Thus, it is plausible that the glucocorticoids produced endogenously by Bat3$^{-/-}$ DCs could act both in an autocrine manner to further reinforce DC regulatory phenotype and in a paracrine manner to suppress T cell responses. Glucocorticoids can drive the expression of Tim-3 on T cells and the development of T cell exhaustion (22). Whereas loss of Tim-3 promotes proinflammatory phenotype in DCs by inducing activation of inflammasome (10), loss of the Tim-3 adapter protein Bat3 promotes a regulatory phenotype in DCs. Therefore, it is possible that the regulatory phenotype observed in Bat3-deficient DCs is due to excessive glucocorticoid production in these DCs, which further leads to induction of Tim-3 signaling in adjacent T cells, thus providing an unexpected expansion to what is known about the Tim-3–Bat3 axis in regulating T cell responses (12). It is plausible that glucocorticoids can also induce or augment the expression of Tim-3 in DCs, which has been reported to restrain the activation of DC by innate stimuli (64), the production of chemokines by DC (65), and activation of the inflammasome in DCs (10). Therefore, the regulatory phenotype observed in Bat3-deficient DCs could be due to unopposed Tim-3 signaling resulting in excessive glucocorticoid production. Further investigation involving Tim-3–Bat3 double-deficient DCs is needed to confirm whether the regulatory function observed in Bat3-deficient DCs is partly due to unopposed Tim-3 signaling.

Activation of UPR-related pathways in DCs subsequent to ER stress can modulate DC functions in multiple ways. First, the levels/ duration of ER stress and UPR activation may tune DC functions differently depending on context. Constitutive activation of IRE1α is observed in DCs when using ER stress–activated indicator reporter mice (66–68), indicating that a baseline level of UPR may be critical for DC development and survival. Overexpression of XBP1s in DCs potentiates the efficacy of DC-based therapeutic cancer

vaccinees (69). Consistent with this observation, pharmacological blockade of the IRE1α/Xbp1 axis in BMDCs impairs antigen cross-presentation (70). However, during progression of ovarian cancer, sustained activation of XBP1s in tumor-infiltrating DCs enhanced abnormal lipid accumulation and inhibited subsequent DC antigen presentation to support activation of antitumor T cells (56). This observation is in line with our observation that Bat3 deficiency resulting from excessive and sustained activation of UPR may have detrimental effects on DCs in priming $CD8^+$ T cells in the implanted MC38-OVA^{dim} tumor models. Second, the different arms of the UPR may have different effects in DCs. Loss of XBP1, but not the other arms of the UPR, results in an increased sensitivity to apoptotic cell death during DC differentiation, resulting in impaired survival of DCs (71). Activation of the protein kinase R-like ER kinase (PERK) pathway and C/EBP homologous protein (CHOP) pathway (72), and IRE1α pathways of the UPR increases IL-23 expression in TLR- activated DCs (73, 74). Although the contribution of different arms of UPR pathways in the generation and function of tolDCs has not been studied, our results indicate that Bat3-mediated regulation of glucocorticoid-GR signaling via the UPR may represent a major component of the regulatory effect observed in Bat3-deficient DCs.

The level of Bat3 in DCs is tightly regulated by the type of stimulus received by these cells, implying a broad yet versatile function of Bat3 in DCs in various disease settings. Our data show that activating or inhibitory signals provided by the environment affect the endogenous Bat3 levels in DC and subsequently their functions. Although the mechanism by which this is achieved is not clear, we hypothesize that activating versus tolerogenic signals may regulate Bat3 expression by (i) inducing transcription factors that regulate Bat3 expression, (ii) activating signaling pathways that regulate Bat3 nuclear translocation, and/or (iii) changing the metabolic status of DCs. Further studies will be needed to identify the precise signaling pathways and the transcription factors that regulate the expression of Bat3 in response to environmental cues.

Collectively, our findings define an endogenous regulator that acts as a molecular switch of DC phenotype and function by regulating ER stress and cellular metabolism by promoting increased steroidogenesis. We showed that in the absence of Bat3, acetyl-CoA was preferentially used for increased steroidogenesis, thereby promoting a regulatory program in T cells. We have thus identified a targetable immunoregulatory program that can be exploited to modulate DC function (immunostimulatory or regulatory) and the subsequent cross-talk between DCs and the T cells in different disease settings. As previously mentioned, DC-based therapy has great potential clinically; however, it has not been used to its full potential due to the plasticity and instability of DCs in vivo. Our study has revealed that Bat3, the adaptive protein of Tim-3, plays a fundamental role in regulating the phenotype of DCs.

MATERIALS AND METHODS

Study design

The aim of this study was to determine the role of Bat3 in DC function. We used mice bearing conditional deletion of Bat3 in DCs (Bat3 cKO) to examine its role in murine models of autoimmunity and cancer. We performed bulk RNA-seq and scRNA-seq to

examine DC and T cell states in Bat3 cKO versus control mice. Bioinformatic analyses led to the investigation of the role of glucocorticoid signaling, ER stress, and the UPR in the phenotypes observed in Bat3 cKO mice. We used GR-deficient mice, ER stress inhibitors, and XBP1 and Bat3 double KO mice to establish the mechanism by which Bat3 exerts its effects in vitro and in vivo. Gene expression was analyzed by qPCR, and protein expression was analyzed by flow cytometry and Western blot. Steroid production was measured using enzyme-linked immunosorbent assay (ELISA). The extent of CNS autoimmunity was scored on a standard scale as detailed in the methods. Tumor size was measured in two dimensions and reported as tumor area. Sample size and replicates are indicated in the figure legends. Details regarding experimental and bioinformatic methods are included below.

Mice

WT C57BL/6, *OT-I*, *OT-II*, *CD11c*^{CRE}, *Nr3c1*$^{fl/fl}$, and *dLck*^{CRE} mice were purchased from the Jackson Laboratory (Bar Harbor, ME). *Bat3*$^{fl/fl}$ mice were a gift from T. W. Mak (Princess Margaret Cancer Centre, Canada) and H. Okada (Kindai University, Japan). *Xbp1*$^{fl/fl}$ mice were provided by L. H. Glimcher (Dana Farber Cancer Institute) (56) and R. Blumberg (Brigham and Women's Hospital) (75). 2D2 mice were created as described previously (24). All mouse strains were maintained in the Brigham and Women's Hospital facility under specific pathogen–free conditions in accordance with institutional guidelines and ethical regulations. All animal work was conducted according to guidelines approved by Institutional Animal Care and Use Committee of Brigham and Women's Hospital. All mice used were sex- and age-matched (6 to 10 weeks old). Littermate WT mice were used as controls.

Experimental autoimmune encephalomyelitis

Active EAE was induced as previously described (12). Equivalent of 50 μg of $MOG_{35–55}$ (MEVGWYRSPFSRVVHLYRNGK) was emulsified in complete Freund's adjuvant (BD Biosciences) containing *Mycobacterium tuberculosis* extract H37-Ra (Difco Laboratories) and subcutaneously injected to each mouse. Immunized mice received pertussis toxin (List Biological Laboratories) on days 0 and 2. Animals were monitored as previously published (12): 0, no disease; 1, decreased tail tone; 2, hind limb weakness or partial paralysis; 3, complete hind limb paralysis; 4, front and hind limb paralysis; 5, moribund state. The brain and spinal cord were harvested at indicated time for flow cytometry analysis and for histopathology analysis at 28 days after immunization.

2D2 naïve T cells transfer in EAE

For 2D2 transfer experiments, 1×10^5 sorted 2D2 naïve cells ($CD4^+CD44^-CD25^-CD62L^+$) were transferred intravenously 1 day before immunization with MOG peptide. Immunization procedures were described above. Mice were euthanized at day 7 for analysis of dLN or when their EAE score reached 2 or 3 (~ day 15) to analyze the infiltrating lymphocytes in the CNS.

Tumor models

Bat3$^{fl/fl}$CD1c^{cre}, *Bat3*$^{fl/fl}$, or WT C57BL/6 mice were subcutaneously injected on the right flank on day 0 with MC38 (5×10^5 cells per mice) or MC38-OVA (2×10^5 cells per mice) cells. The size of the tumor was monitored and quantified as reported (22). Tumor size was calculated using the formula $L \times W$, where L is the longest dimension and W is the shortest perpendicular dimension. The measures were performed in blinded manner. All mice were euthanized before the tumor size exceeded 400 mm^2.

Intratumoral treatment

The mice with the same genotypes were randomized into different groups based on the tumor size before treatment. 4PBA (100 μg) in 50 μl of vehicle was injected intratumorally starting on an average tumor size of about 40 mm^2 (days 6 and 8) in *Bat3*$^{fl/fl}$CD1c^{CRE} and *Bat3*$^{fl/fl}$ mice.

BMDC cell culture

BMDCs were prepared from the femurs and tibiae of mice 6 to 12 weeks of age. For granulocyte-macrophage colony-stimulating factor (GM-CSF)–differentiated BMDCs, cells were cultured in RPMI 1640 medium (Sigma-Aldrich) with 10% fetal bovine serum (Thermo Fisher Scientific), 50 μM β-mercaptoethanol (Sigma-Aldrich), and 2 mM L-glutamine, penicillin (100 U/ml), streptomycin (100 mg/ml) (penicillin-streptomycin), 12 mM Hepes, and GM-CSF (20 ng/ml; PeproTech). BMDCs were treated with LPS (500 ng/ml), and the indicated concentration of 4PBA (Sigma-Aldrich) and 4μ8C (Millipore) was treated for 8 hours. Reagents were added to cells simultaneously with LPS. To differentiate DCs for the DC-based therapy in the tumor experiments, bone marrow cells were plated at 2×10^6 cells per well in DC medium with Flt3L (100 ng/ml) in six-well plates and cultured at 37°C in a humidified atmosphere at 10% CO_2. OP9 cell lines were cultured in minimum essential medium–α medium supplemented with 20% fetal bovine serum and 1% penicillin-streptomycin (OP9 medium) at 37°C in a humidified atmosphere at 5% CO_2. Before using in cocultures, OP9 cells were radiated for 15 min. On day 3 of differentiation, cells from each well were transferred to a single well containing a monolayer of radiated OP9 cells in 10-cm plates. DCs were harvested and sorted on day 7. Using this method, we obtained a mixture of CD11b$^+$ DCs and CD103$^+$ DCs with a ratio of about 3:1 (76).

BMDC transfer in the EAE and tumor model

After immunization with MOG peptide, mice were divided randomly into different groups. BMDCs (10×10^6) with different genotypes or treatment were given subcutaneously, respectively, to each mouse at 0 and 3 days after immunization. BMDCs were treated with 4PBA (10 μM) or 4μ8C (2 μM) for 8 hours before transfer. For the DC-based therapy studies in tumor model, cultured DCs were subcutaneously injected on the inguinal lymph node (iLN) right side adjacent to the tumor at a tumor size of about 5 mm by 5 mm. A total of 2×10^6 sorted, live CD11c$^+$ MHC-II$^+$ cells were transferred per mice.

T cell culture and treatment with glucocorticoid

$CD4^+$ T cells or $CD8^+$ T cells from splenocytes and lymph nodes were isolated using microbeads (Miltenyi Biotec). $CD4^+CD25^-CD62L^{hi}$ $CD44^-$ and $CD8^+CD25^-CD62L^{hi}CD44^-$ naïve cells were sorted by BD FACSAria (BD Biosciences) and cultured for 9 days as previously described (22). Briefly, naïve cells were stimulated with plate-bound anti-CD3 (145–2C11; 1 μg/ml) and anti-CD28 (PV-1; 1 μg/ml) in the presence of 100 nM corticosterone (Thermo Fisher Scientific) for 3 days. Cells were then rested in the presence of IL-2 (5 ng/ml; Miltenyi Biotec) for 3 days, followed by restimulation with plate-bound anti-CD3 (145–2C11; 1 μg/ml) and anti-CD28 (PV-1; 1 μg/ml) in the presence of 100 nM corticosterone (Thermo Fisher Scientific) for an additional 3 days.

Histopathological analysis

At end point of day 28, brains and spinal cords were fixed in 10% neutral-buffered formalin and processed routinely for paraffin embedment. Slides were stained with hematoxylin and eosin stains. Inflammatory foci (>10 mononuclear cells) were counted in leptomeninges and parenchyma in a blinded fashion.

Isolation of mononuclear cells from disease models

Mononuclear cells were isolated from the iLN or CNS at the indicated time of EAE. Mice were euthanized and were immediately perfused with ice-cold phosphate-buffered saline. In CNS tissues, dLNs were harvested as reported (12). Tumors were collected for analysis on day 12. These homogenized tissues were digested with collagenase D (2.5 mg/ml; Roche) and deoxyribonuclease I (1 mg/ml; Sigma-Aldrich) at 37°C for 30 min. Tumors were mechanically disrupted with gentle magnetic cell sorter (MACS) C-tubes and dissociator (Miltenyi Biotec). Mononuclear cells were isolated on a discontinuous Percoll gradient (GE Healthcare), 30%/70% Percoll for CNS tissues; harvested the interface, 33, 47, and 63% Percoll for tumor tissues; and harvested both interfaces. Isolated cells were then used in various downstream assays. To assess cytokine production, cells were incubated in clone medium containing phorbol 12-myristate 13-acetate (50 ng/ml) and ionomycin (500 ng/ml) with GolgiPlug and GolgiStop (BD Biosciences) at 37°C with 10% CO_2 for 4 hours. In particular, for CD107a staining of TILs, antibody against CD107a (1D4B) was added to the culture medium during stimulation. For isolation of DCs, tissues (spleen, CNS, dLN, or tumor) were harvested and digested in digestion buffer mentioned above. cDCs were defined as $CD3^-CD19^-NK1.1^-Ly6C^-Ly6G^-F4/80^-$Siglec F^-CD11c^+MHC-II^+ cells (further separated by $CD11b^+$ as cDC2, $CD103^+$ in nonlymphoid, or $CD8a^+$ in lymphoid tissue as cDC1) and were sorted using Aria cell sorter (BD Biosciences). The following antibodies were used for surface staining (from BioLegend unless otherwise specified): CD3ε (145–2C11), CD4 (RM4–5), CD8α (53–6.7), CD11b (M1/70), CD11c (HL3 for staining the CD11c+ cells enriched by MACS beads and N418 for other purpose), CD19 (534 6D5), CD44 (IM7), CD45 (30-F11), CD64 (X54–5/7.1), CD107a (1D4B), B220 (RA3–6B2), F4/80 (BM8), I-A/I-E (M5/114.15.2), Ly6C (HK1.4), Ly6G (1A8; BD), NK1.1 (PK136), Siglec F (E50–2440; BD), TCR Va3.2 (RR3–16), TCRβ (H57–597), and Tim-3 (5D12).

DC–T cell coculture assays

For antigen presentation experiments, the total $CD4^+$ T or $CD8^+$ T cells were enriched with MACS beads and columns (Miltenyi Biotec). Naïve T cells were labeled and sorted as $CD25^-CD44^-CD62L^+$ from 2D2, OT-I, or OT-II mice. The sorted naïve T cells were labeled with CellTrace Violet before coculture (Thermo Fisher Scientific). BMDCs were pretreated with LPS (500 μg/ml) or ER stress modulators 4PBA (5 μM) or 4μ8C (5 μM) for 8 hours before coculture. The live $CD11c^{hi}$ BMDCs, ex vivo splenic DCs (DC2, $CD11c^{hi}MHC\text{-}II^+CD64^-CD11b^+$; or DC1, $CD11c^{hi}MHC\text{-}II^+CD64^-CD8\alpha^+$), or tDCs (DC2, $CD11c^{hi}MHC\text{-}II^+CD64^-CD24^+CD11b^+$; or DC1, $CD11c^{hi}MHC\text{-}II^+CD64^-CD24^+CD103^+$) were sorted and incubated with antigens for 4 hours. After incubation, DCs were washed twice with medium before proceeding to coculture with T cells at 1:10 (BMDC to T cell ratio) or 1:40 (splenic DC to T cell ratio) in clone medium for 72 hours. In nonantigen-specific studies, BMDCs and naïve T cell were cocultured in the presence of soluble anti-CD3 in void of antigen.

Flow cytometry analysis

For flow cytometric analysis, cells were stained with e506 LIVE/DEAD fixable dye (eBioscience) or 7-aminoactinomycin D (7-AAD) (BD Pharmigen) for 10 min on ice. Pelleted cells were incubated with Fc blocker (BioLegend) or normal mouse immunoglobulin G (IgG) (Life Technologies) for 10 min on ice to block the binding to Fc receptors. Extracellular antigens were stained for 20 min with antibodies on ice in a staining buffer. Cells were fixed and permeabilized with BD Cytofix/Cytoperm (for cytokine analysis) or eBioscience Transcription Factor Fix/Perm (for Bat3 or FoxP3 analysis) per the manufacturers' instructions. Intracellular antigens were stained for 45 min on ice in the appropriate 1× perm/wash buffer before acquisition on a BD LSR II/Fortessa/Symphony flow cytometer (Becton Dickinson). The following antibodies were used (BioLegend unless otherwise specified): Bat3 (EPR9223, Abcam), anti-BrdU (3D4), FoxP3 (FJK-16, eBioscience), Granzyme B (QA16A02), IFN-γ (XMG1.2), IL-17A (Tc11–538 18H10.1), IL-10 (JES5–16E3), IL-2 (JES6–5H4), and TNF-α (MP6-XT22). Negative staining was determined using the appropriate isotype control antibody or Fluorescence Minus One control. Counting beads (BioLegend) were added to quantify absolute cell numbers. Results were acquired with the Diva software and analyzed using FlowJo software (Treestar).

Western blot analysis

Whole-cell lysates, cytoplasmic, organellular/membrane, and nuclear/cytoskeletal fractions were isolated using the Cell Fractionation Kit [Cell Signaling Technology (CST)]. Protein concentration was determined using the bicinchoninic acid (BCA) protein assay to standardize protein concentration and equalize before loading (Pierce). Equivalent amounts of samples (usually 30 to 40 μg) were separated via Bolt Bis-Tris Plus Gels (Invitrogen) and transferred onto nitrocellulose membranes (Thermo Fisher Scientific) by Power Blotter 1-Step Transfer system (Invitrogen). After blocking, the membrane was incubated with primary antibodies overnight at 4°C. The following antibodies were used for Western blot: anti-histone H3 (clone: D1H2, CST) and XBP1s (clone: D2C1F, CST). The blots were

incubated with anti-rabbit IgG and horseradish peroxidase–linked antibody (CST) at 20°C for 30 min. Last, the membranes were detected using Western blot film developer (Kodak).

Conventional and real-time PCR

Total RNA was extracted from target cells using Picoure reagents (Thermo Fisher Scientific), and reverse transcription was done with iScript Reverse Transcriptase (Bio-Rad). Real-time PCR was performed in the Vii7 Real-Time PCR system (Applied Biosystems) using validated primer-probe sets (Thermo Fisher Scientific, catalog numbers were listed in table S1), the appropriate endogenous control β-actin (mouse)–probe sets (Thermo Fisher Scientific, catalog no. 4352341E). Primer sequences are listed in table S1. TaqMan FAST mix or with SYBR Green–based qPCR was used according to the manufacturer's instruction (all Applied Biosystems). Data were normalized to the expression of Actb. *Xbp1* splicing assays were performed as previously described (77) using conventional reverse transcription PCR.

Metabolite measurements

Supernatant of cell culture were subjected to examination of corticosterone (Arbor Assays) using ELISA. The acetyl-CoA, fumarate, citrate, and cholesterol were determined on total or cytosolic fractions using the PicoProbe Acetyl-CoA (BioVision), Fumarate Assay Kit (BioVision), Citrate Assay Kit (BioVision), and Cholesterol/Cholesteryl Ester Quantitation Kit (BioVision), respectively, according to the manufacturer's instructions.

Bulk RNA-seq

Biological replicates of equal cell numbers from BMDCs with indicated conditions as mentioned in the figure captions were used to sort directly into TCL buffer (QIAGEN) for generating the RNA sample for each group. This was followed by first-strand cDNA synthesis using random hexamer-primer, which was followed by adding a buffer containing deoxynucleoside triphosphates, ribonuclease H, and DNA polymerase I to synthesize the second strand. The generated double-stranded cDNA was then purified with magnetic beads (Thermo Fisher Scientific) and the end reparation, and 3′-end single-nucleotide A (adenine) addition was then performed. Thereafter, sequence adaptors were ligated to the fragments, which were later enriched by PCR amplification. After the quality control step, library products were ready for RNA-seq. Raw sequencing images from the flowcell were demultiplexed using the Illumina bcl2fastq command. The resulting fastq files were aligned to the mouse reference genome (mm10) using the STAR genome aligner (78), and transcripts were quantified using RSEM (79) and aggregated at the level of genes. Gene counts were subjected to differential expression analysis using the R package DESeq2 (80) (or EdgeR for only the public dataset), followed by prioritization of genes at an FDR of <0.05. Pathway enrichment analysis was performed on the prioritized genes using the hypergeometric framework in Homer (81).

Droplet-based scRNA-seq

T cells ($CD45^{hi}$ $CD3^{+}$ $CD4^{+}$ and $CD45^{hi}$ $CD3^{+}$ $CD8^{+}$) were sorted and pooled from five EAE mice with the same experimental group. Single-cell suspensions were loaded onto

3′ library chips for the Chromium Single Cell 3′ Library (v3, PN-1000269) according to the manufacturer's recommendations (10X Genomics). An input of 10,000 single cells was added to each channel with a recovery rate of about 4000 cells per channel. Libraries were sequenced on an Illumina NextSeq 500. Sequencing files were demultiplexed (cellranger makefastq), aligned to the mm10 genome reference, and quantified to gene level counts (cellranger count) using the 10X Cell Ranger software. Data analysis was performed using the Seurat (v3) R package. Only cells with at least 200 genes were detected, and a fraction of mitochondrial reads fewer than 50% were retained for downstream analysis. Cell gene expression was normalized (NormalizeData), followed by identification of highly variable genes (FindVariableFeatures). Dimensionality reduction was performed using principal components analysis ($k = 50$) on the scaled dataset (ScaleData), followed by graph-based clustering [FindNeighbors ($k = 50$) and FindClusters] at a resolution of 1. Cells were embedded in uniform manifold approximation and projection (UMAP) (FindUMAP) space for visualization. Cluster identity genes were identified using the Wilcoxon rank sum test (FindAllMarkers). The R package dplyr (82), ggplot2 (83), cowplot (84), and pheatmap (85) were used for visualizing. The UpsetR package (86) was used to quantify the intersection of regulatory gene programs.

Statistics

Data are presented as means ± SEM. Student's *t* test was used for statistical evaluation for two-group comparison in normally distributed data. For more than two groups, data were analyzed by one-way analysis of variance (ANOVA) or two-way ANOVA, followed by Tukey's post hoc tests for multiple comparisons. Disease incidence data were analyzed using Fisher's exact test. Maximal disease scores were analyzed using the Mann-Whitney *U* test. To assess the differential onset of disease or tumor growth between different groups, linear regression analysis was performed to determine the slope of disease onset. All *P* values are two-sided, and statistical significance was assessed at the 0.05 level.

Supplementary Material

Refer to Web version on PubMed Central for supplementary material.

Acknowledgments:

We thank all members of the Kuchroo Laboratory, Anderson Laboratory, and R. Blumberg for discussions; D. Kozoriz and R. K. Krishnan for cell sorting; L. Nguyen and D. Dionne for RNA-seq; M. Singer and S. Riesenfeld for computational advice; L. Gaffney for figure preparation; and M. Collins and G. Escobar for careful reading of the manuscript.

V.K.K. has an ownership interest and is a member of the SAB of Celsius Therapeutics, Tizona Therapeutics, Trishula Therapeutics, Werewolf Therapeutics, and Larkspur Biosciences. A.C.A. is a member of the SAB for Tizona Therapeutics, Trishula Therapeutics, Compass Therapeutics, Zumutor Biologics, and ImmuneOncia, which have interests in cancer immunotherapy. A.C.A. is also a paid consultant for iTeos Therapeutics and Larkspur Biosciences. V.K.K.'s and A.C.A.'s interests were reviewed and managed by the Brigham and Women's Hospital and Partners Healthcare in accordance with their conflict-of-interest policies. A.R. is a cofounder and equity holder of Celsius Therapeutics, an equity holder in Immunitas Therapeutics, and an SAB member of Thermo Fisher Scientific and Syros Pharmaceuticals as well as Neogene Therapeutics until 1 August 2020. From 1 August 2020, A.R. is an employee of Genentech. A.R. is a named inventor on several patents and patent applications filed by the Broad Institute in the area of single cell and spatial genomics.

Funding:

The study is supported by grants P01AI039671, P01AI056299, R01AI144166, and P01AI073748 granted to V.K.K. and R01CA229400 granted to A.C.A. by the National Institutes of Health. A.C.A. is a recipient of the Brigham and Women's Hospital President's Scholar Award. Additional supports come from the Klarman Cell Observatory at the Broad Institute, Klarman Incubator Funds at the Broad Institute and the Howard Hughes Medical Institute.

Data and materials availability:

The data generated for this study have been deposited in the GEO database (GSE169664). The vitamin D3-induced regulatory DC bulk RNA-seq dataset (87) was received from the authors directly on personal communication.

REFERENCES AND NOTES

1. Durai V, Murphy KM, Functions of murine dendritic cells. Immunity 45, 719–736 (2016). [PubMed: 27760337]
2. Merad M, Sathe P, Helft J, Miller J, Mortha A, The dendritic cell lineage: Ontogeny and function of dendritic cells and their subsets in the steady state and the inflamed setting. Annu. Rev. Immunol 31, 563–604 (2013). [PubMed: 23516985]
3. Cabeza-Cabrerizo M, Cardoso A, Minutti CM, Pereira da Costa M, Reis E Sousa C, Dendritic cells revisited. Annu. Rev. Immunol 39, 131–166 (2021). [PubMed: 33481643]
4. C. A. Iberg, A. Jones, D. Hawiger, Dendritic cells as inducers of peripheral tolerance. Trends Immunol. 38, 793–804 (2017). [PubMed: 28826942]
5. Benham H, Nel HJ, Law SC, Mehdi AM, Street S, Ramnoruth N, Pahau H, Lee BT, Ng J, Brunck ME, Hyde C, Trouw LA, Dudek NL, Purcell AW, O'Sullivan BJ, Connolly JE, Paul SK, Lê Cao KA, Thomas R, Citrullinated peptide dendritic cell immunotherapy in HLA risk genotype-positive rheumatoid arthritis patients. Sci. Transl. Med 7, 290ra287 (2015).
6. Giannoukakis N, Phillips B, Finegold D, Harnaha J, Trucco M, Phase I (safety) study of autologous tolerogenic dendritic cells in type 1 diabetic patients. Diabetes Care 34, 2026–2032 (2011). [PubMed: 21680720]
7. Wculek SK, Cueto FJ, Mujal AM, Melero I, Krummel MF, Sancho D, Dendritic cells in cancer immunology and immunotherapy. Nat. Rev. Immunol 20, 7–24 (2020). [PubMed: 31467405]
8. Chang CC, Ogino T, Mullins DW, Oliver JL, Yamshchikov GV, Bandoh N, Slingluff CL, Ferrone S, Defective human leukocyte antigen class I-associated antigen presentation caused by a novel beta2-microglobulin loss-of-function in melanoma cells. J. Biol. Chem 281, 18763–18773 (2006). [PubMed: 16648140]
9. Bennaceur K, Chapman J, Brikci-Nigassa L, Sanhadji K, Touraine JL, Portoukalian J, Dendritic cells dysfunction in tumour environment. Cancer Lett. 272, 186–196 (2008). [PubMed: 18585853]
10. Dixon KO, Tabaka M, Schramm MA, Xiao S, Tang R, Dionne D, Anderson AC, Rozenblatt-Rosen O, Regev A, Kuchroo VK, TIM-3 restrains anti-tumour immunity by regulating inflammasome activation. Nature 595, 101–106 (2021). [PubMed: 34108686]
11. de Mingo Pulido Á, Hänggi K, Celias DP, Gardner A, Li J, Batista-Bittencourt B, Mohamed E, Trillo-Tinoco J, Osunmakinde O, Peña R, Onimus A, Kaisho T, Kaufmann J, McEachern K, Soliman H, Luca VC, Rodriguez PC, Yu X, Ruffell B, The inhibitory receptor TIM-3 limits activation of the cGAS-STING pathway in intra-tumoral dendritic cells by suppressing extracellular DNA uptake. Immunity 54, 1154–1167.e7 (2021). [PubMed: 33979578]
12. Rangachari M, Zhu C, Sakuishi K, Xiao S, Karman J, Chen A, Angin M, Wakeham A, Greenfield EA, Sobel RA, Okada H, McKinnon PJ, Mak TW, Addo MM, Anderson AC, Kuchroo VK, Bat3 promotes T cell responses and autoimmunity by repressing Tim-3–mediated cell death and exhaustion. Nat. Med 18, 1394–1400 (2012). [PubMed: 22863785]
13. Spies T, Blanck G, Bresnahan M, Sands J, Strominger JL, A new cluster of genes within the human major histocompatibility complex. Science 243, 214–217 (1989). [PubMed: 2911734]

14. Banerji J, Sands J, Strominger JL, Spies T, A gene pair from the human major histocompatibility complex encodes large proline-rich proteins with multiple repeated motifs and a single ubiquitin-like domain. Proc. Natl. Acad. Sci. U.S.A 87, 2374–2378 (1990). [PubMed: 2156268]
15. Hsieh YY, Lin YJ, Chang CC, Chen DY, Hsu CM, Wang YK, Hsu KH, Tsai FJ, Human lymphocyte antigen B-associated transcript 2, 3, and 5 polymorphisms and haplotypes are associated with susceptibility of Kawasaki disease and coronary artery aneurysm. J. Clin. Lab. Anal 24, 262–268 (2010). [PubMed: 20626023]
16. Degli-Esposti MA, Abraham LJ, McCann V, Spies T, Christiansen FT, Dawkins RL, Ancestral haplotypes reveal the role of the central MHC in the immunogenetics of IDDM. Immunogenetics 36, 345–356 (1992). [PubMed: 1356098]
17. Harney SM, Vilariño-Güell C, Adamopoulos IE, Sims AM, Lawrence RW, Cardon LR, Newton JL, Meisel C, Pointon JJ, Darke C, Athanasou N, Wordsworth BP, Brown MA, Fine mapping of the MHC Class III region demonstrates association of AIF1 and rheumatoid arthritis. Rheumatology 47, 1761–1767 (2008). [PubMed: 18835879]
18. Piras IS, Angius A, Andreani M, Testi M, Lucarelli G, Floris M, Marktel S, Ciceri F, La Nasa G, Fleischhauer K, Roncarolo MG, Bulfone A, Gregori S, Bacchetta R, BAT2 and BAT3 polymorphisms as novel genetic risk factors for rejection after HLA-related SCT. Bone Marrow Transplant. 49, 1400–1404 (2014). [PubMed: 25111513]
19. Etokebe GE, Zienolddiny S, Kupanovac Z, Enersen M, Balen S, Flego V, Bulat-Kardum L, Radojčić-Badovinac A, Skaug V, Bakke P, Haugen A, Dembic Z, Association of the FAM46A gene VNTRs and BAG6 rs3117582 SNP with non small cell lung cancer (NSCLC) in Croatian and Norwegian populations. PLOS ONE 10, e0122651 (2015).
20. Zhao J, Wang H, Hu W, Jin Y, Effect of HLA-B-associated transcript 3 polymorphisms on lung cancer risk: A meta-analysis. Med. Sci. Monit 20, 2461–2465 (2014). [PubMed: 25430685]
21. Zhu C, Dixon KO, Newcomer K, Gu G, Xiao S, Zaghouani S, Schramm MA, Wang C, Zhang H, Goto K, Christian E, Rangachari M, Rosenblatt-Rosen O, Okada H, Mak T, Singer M, Regev A, Kuchroo V, Tim-3 adaptor protein Bat3 is a molecular checkpoint of T cell terminal differentiation and exhaustion. Sci. Adv 7, (2021).
22. Acharya N, Madi A, Zhang H, Klapholz M, Escobar G, Dulberg S, Christian E, Ferreira M, Dixon KO, Fell G, Tooley K, Mangani D, Xia J, Singer M, Bosenberg M, Neuberg D, Rozenblatt-Rosen O, Regev A, Kuchroo VK, Anderson AC, Endogenous glucocorticoid signaling regulates $CD8^+$ T cell differentiation and development of dysfunction in the tumor microenvironment. Immunity 53, 658–671.e6 (2020). [PubMed: 32937153]
23. Sakuishi K, Apetoh L, Sullivan JM, Blazar BR, Kuchroo VK, Anderson AC, Targeting Tim-3 and PD-1 pathways to reverse T cell exhaustion and restore anti-tumor immunity. J. Exp. Med 207, 2187–2194 (2010). [PubMed: 20819927]
24. Bettelli E, Baeten D, Jäger A, Sobel RA, Kuchroo VK, Myelin oligodendrocyte glycoprotein-specific T and B cells cooperate to induce a Devic-like disease in mice. J. Clin. Invest 116, 2393–2402 (2006). [PubMed: 16955141]
25. Joffre O, Nolte MA, Spörri R, Reis e Sousa C, Inflammatory signals in dendritic cell activation and the induction of adaptive immunity. Immunol. Rev 227, 234–247 (2009). [PubMed: 19120488]
26. Xia CQ, Peng R, Beato F, Clare-Salzler MJ, Dexamethasone induces IL-10-producing monocyte-derived dendritic cells with durable immaturity. Scand. J. Immunol 62, 45–54 (2005). [PubMed: 16091124]
27. Piemonti L, Monti P, Allavena P, Sironi M, Soldini L, Leone BE, Socci C, Di Carlo V, Glucocorticoids affect human dendritic cell differentiation and maturation. J. Immunol 162, 6473–6481 (1999). [PubMed: 10352262]
28. Piemonti L, Monti P, Sironi M, Fraticelli P, Leone BE, Dal Cin E, Allavena P, Di Carlo V, Vitamin D3 affects differentiation, maturation, and function of human monocyte-derived dendritic cells. J. Immunol 164, 4443–4451 (2000). [PubMed: 10779743]
29. De Smedt T, Van Mechelen M, De Becker G, Urbain J, Leo O, Moser M, Effect of interleukin-10 on dendritic cell maturation and function. Eur. J. Immunol 27, 1229–1235 (1997). [PubMed: 9174615]

30. Gonzalez-Rey E, Chorny A, Fernandez-Martin A, Ganea D, Delgado M, Vasoactive intestinal peptide generates human tolerogenic dendritic cells that induce CD4 and CD8 regulatory T cells. Blood 107, 3632–3638 (2006). [PubMed: 16397128]

31. Bakdash G, Vogelpoel LT, van Capel TM, Kapsenberg ML, de Jong EC, Retinoic acid primes human dendritic cells to induce gut-homing, IL-10-producing regulatory T cells. Mucosal Immunol. 8, 265–278 (2015). [PubMed: 25027601]

32. Monti P, Mercalli A, Leone BE, Valerio DC, Allavena P, Piemonti L, Rapamycin impairs antigen uptake of human dendritic cells. Transplantation 75, 137–145 (2003). [PubMed: 12544886]

33. Buckland M, Jago C, Fazekesova H, George A, Lechler R, Lombardi G, Aspirin modified dendritic cells are potent inducers of allo-specific regulatory T-cells. Int. Immunopharmacol 6, 1895–1901 (2006). [PubMed: 17219690]

34. Tajima K, Amakawa R, Ito T, Miyaji M, Takebayashi M, Fukuhara S, Immunomodulatory effects of cyclosporin A on human peripheral blood dendritic cell subsets. Immunology 108, 321–328 (2003). [PubMed: 12603598]

35. Chen T, Guo J, Yang M, Han C, Zhang M, Chen W, Liu Q, Wang J, Cao X, Cyclosporin A impairs dendritic cell migration by regulating chemokine receptor expression and inhibiting cyclooxygenase-2 expression. Blood 103, 413–421 (2004). [PubMed: 14504089]

36. Okunishi K, Dohi M, Nakagome K, Tanaka R, Mizuno S, Matsumoto K, Miyazaki J, Nakamura T, Yamamoto K, A novel role of hepatocyte growth factor as an immune regulator through suppressing dendritic cell function. J. Immunol 175, 4745–4753 (2005). [PubMed: 16177122]

37. Cannarile L, Delfino DV, Adorisio S, Riccardi C, Ayroldi E, Implicating the role of GILZ in glucocorticoid modulation of T-cell activation. Front. Immunol 10, 1823 (2019). [PubMed: 31440237]

38. Varricchio L, Migliaccio AR, The role of glucocorticoid receptor (GR) polymorphisms in human erythropoiesis. Am. J. Blood Res 4, 53–72 (2014). [PubMed: 25755906]

39. Wang C, Nanni L, Novakovic B, Megchelenbrink W, Kuznetsova T, Stunnenberg HG, Ceri S, Logie C, Extensive epigenomic integration of the glucocorticoid response in primary human monocytes and in vitro derived macrophages. Sci. Rep 9, 2772 (2019). [PubMed: 30809020]

40. Chen Y, Wang J, Wang X, Li X, Song J, Fang J, Liu X, Liu T, Wang D, Li Q, Wen S, Ma D, Xia J, Luo L, Zheng SG, Cui J, Zeng G, Chen L, Cheng B, Wang Z, Pik3ip1 is a negative immune regulator that inhibits antitumor T-cell immunity. Clin. Cancer Res 25, 6180–6194 (2019). [PubMed: 31350312]

41. Murter B, Kane LP, Control of T lymphocyte fate decisions by PI3K signaling. F1000Res. 9, (2020).

42. Uche UU, Piccirillo AR, Kataoka S, Grebinoski SJ, D'Cruz LM, Kane LP, PIK3IP1/TrIP restricts activation of T cells through inhibition of PI3K/Akt. J. Exp. Med 215, 3165–3179 (2018). [PubMed: 30429249]

43. Piovan E, Yu J, Tosello V, Herranz D, Ambesi-Impiombato A, Da Silva AC, Sanchez-Martin M, Perez-Garcia A, Rigo I, Castillo M, Indraccolo S, Cross JR, de Stanchina E, Paietta E, Racevskis J, Rowe JM, Tallman MS, Basso G, Meijerink JP, Cordon-Cardo C, Califano A, Ferrando AA, Direct reversal of glucocorticoid resistance by AKT inhibition in acute lymphoblastic leukemia. Cancer Cell 24, 766–776 (2013). [PubMed: 24291004]

44. Akahane T, Sahara K, Yashiroda H, Tanaka K, Murata S, Involvement of Bag6 and the TRC pathway in proteasome assembly. Nat. Commun 4, 2234 (2013). [PubMed: 23900548]

45. Rodrigo-Brenni MC, Gutierrez E, Hegde RS, Cytosolic quality control of mislocalized proteins requires RNF126 recruitment to Bag6. Mol. Cell 55, 227–237 (2014). [PubMed: 24981174]

46. Shao S, Rodrigo-Brenni MC, Kivlen MH, Hegde RS, Mechanistic basis for a molecular triage reaction. Science 355, 298–302 (2017). [PubMed: 28104892]

47. Hessa T, Sharma A, Mariappan M, Eshleman HD, Gutierrez E, Hegde RS, Protein targeting and degradation are coupled for elimination of mislocalized proteins. Nature 475, 394–397 (2011). [PubMed: 21743475]

48. Wang Q, Liu Y, Soetandyo N, Baek K, Hegde R, Ye Y, A ubiquitin ligase-associated chaperone holdase maintains polypeptides in soluble states for proteasome degradation. Mol. Cell 42, 758–770 (2011). [PubMed: 21636303]

49. Mariappan M, Li X, Stefanovic S, Sharma A, Mateja A, Keenan RJ, Hegde RS, A ribosome-associating factor chaperones tail-anchored membrane proteins. Nature 466, 1120–1124 (2010). [PubMed: 20676083]
50. Sarvani C, Sireesh D, Ramkumar KM, Unraveling the role of ER stress inhibitors in the context of metabolic diseases. Pharmacol. Res 119, 412–421 (2017). [PubMed: 28237513]
51. Sanches M, Duffy NM, Talukdar M, Thevakumaran N, Chiovitti D, Canny MD, Lee K, Kurinov I, Uehling D, Al-awar R, Poda G, Prakesch M, Wilson B, Tam V, Schweitzer C, Toro A, Lucas JL, Vuga D, Lehmann L, Durocher D, Zeng Q, Patterson JB, Sicheri F, Structure and mechanism of action of the hydroxy-aryl-aldehyde class of IRE1 endoribonuclease inhibitors. Nat. Commun 5, 4202 (2014). [PubMed: 25164867]
52. Martinez-Reyes I, Chandel NS, Mitochondrial TCA cycle metabolites control physiology and disease. Nat. Commun 11, 102 (2020). [PubMed: 31900386]
53. Pietrocola F, Galluzzi L, Bravo-San Pedro JM, Madeo F, Kroemer G, Acetyl coenzyme A: A central metabolite and second messenger. Cell Metab. 21, 805–821 (2015). [PubMed: 26039447]
54. Del Valle JR, Betts BC, Yu XZ, Janssens S, Lambrecht BN, Simon MC, Hu CA, Clarifying the translational potential of B-I09. Nat. Chem. Biol 16, 1152 (2020). [PubMed: 33067597]
55. Sheng X, Nenseth HZ, Qu S, Kuzu OF, Frahnow T, Simon L, Greene S, Zeng Q, Fazli L, Rennie PS, Mills IG, Danielsen H, Theis F, Patterson JB, Jin Y, Saatcioglu F, IRE1α-XBP1s pathway promotes prostate cancer by activating c-MYC signaling. Nat. Commun 10, 323 (2019). [PubMed: 30679434]
56. Cubillos-Ruiz JR, Silberman PC, Rutkowski MR, Chopra S, Perales-Puchalt A, Song M, Zhang S, Bettigole SE, Gupta D, Holcomb K, Ellenson LH, Caputo T, Lee AH, Conejo-Garcia JR, Glimcher LH, ER stress sensor XBP1 controls anti-tumor immunity by disrupting dendritic cell homeostasis. Cell 161, 1527–1538 (2015). [PubMed: 26073941]
57. Steinbrink K, Wölfl M, Jonuleit H, Knop J, Enk AH, Induction of tolerance by IL-10-treated dendritic cells. J. Immunol 159, 4772–4780 (1997). [PubMed: 9366401]
58. Longman RS, Braun D, Pellegrini S, Rice CM, Darnell RB, Albert ML, Dendritic-cell maturation alters intracellular signaling networks, enabling differential effects of IFN-α/β on antigen cross-presentation. Blood 109, 1113–1122 (2007). [PubMed: 17018853]
59. Gansemer ER, McCommis KS, Martino M, King-McAlpin AQ, Potthoff MJ, Finck BN, Taylor EB, Rutkowski DT, NADPH and glutathione redox link TCA cycle activity to endoplasmic reticulum homeostasis. iScience 23, 101116 (2020).
60. Westerterp M, Gautier EL, Ganda A, Molusky MM, Wang W, Fotakis P, Wang N, Randolph GJ, D'Agati VD, Yvan-Charvet L, Tall AR, Cholesterol accumulation in dendritic cells links the inflammasome to acquired immunity. Cell Metab. 25, 1294–1304.e6 (2017). [PubMed: 28479366]
61. Mailer RKW, Gisterå A, Polyzos KA, Ketelhuth DFJ, Hansson GK, Hypercholesterolemia induces differentiation of regulatory T cells in the liver. Circ. Res 120, 1740–1753 (2017). [PubMed: 28420668]
62. Jaisser F, Farman N, Emerging roles of the mineralocorticoid receptor in pathology: Toward new paradigms in clinical pharmacology. Pharmacol. Rev 68, 49–75 (2016). [PubMed: 26668301]
63. Cain DW, Cidlowski JA, Immune regulation by glucocorticoids. Nat. Rev. Immunol 17, 233–247 (2017). [PubMed: 28192415]
64. Chiba S, Baghdadi M, Akiba H, Yoshiyama H, Kinoshita I, Dosaka-Akita H, Fujioka Y, Ohba Y, Gorman JV, Colgan JD, Hirashima M, Uede T, Takaoka A, Yagita H, Jinushi M, Tumor-infiltrating DCs suppress nucleic acid-mediated innate immune responses through interactions between the receptor TIM-3 and the alarmin HMGB1. Nat. Immunol 13, 832–842 (2012). [PubMed: 22842346]
65. de Mingo Pulido Á, Gardner A, Hiebler S, Soliman H, Rugo HS, Krummel MF, Coussens LM, Ruffell B, TIM-3 regulates CD103^{+} dendritic cell function and response to chemotherapy in breast cancer. Cancer Cell 33, 60–74.e6 (2018). [PubMed: 29316433]
66. Iwakoshi NN, Pypaert M, Glimcher LH, The transcription factor XBP-1 is essential for the development and survival of dendritic cells. J. Exp. Med 204, 2267–2275 (2007). [PubMed: 17875675]

67. Osorio F, Tavernier SJ, Hoffmann E, Saeys Y, Martens L, Vetters J, Delrue I, De Rycke R, Parthoens E, Pouliot P, Iwawaki T, Janssens S, Lambrecht BN, The unfolded-proteinresponse sensor IRE-1α regulates the function of CD8α+ dendritic cells. Nat. Immunol 15, 248–257 (2014). [PubMed: 24441789]
68. Iwawaki T, Akai R, Kohno K, Miura M, A transgenic mouse model for monitoring endoplasmic reticulum stress. Nat. Med 10, 98–102 (2004). [PubMed: 14702639]
69. Tian S, Liu Z, Donahue C, Falo LD, You Z, Genetic targeting of the active transcription factor XBP1s to dendritic cells potentiates vaccine-induced prophylactic and therapeutic antitumor immunity. Mol. Ther 20, 432–442 (2012). [PubMed: 21934655]
70. Medel B, Costoya C, Fernandez D, Pereda C, Lladser A, Sauma D, Pacheco R, Iwawaki T, Salazar-Onfray F, Osorio F, IRE1α activation in bone marrow-derived dendritic cells modulates innate recognition of melanoma cells and favors $CD8^+$ T cell priming. Front. Immunol 9, 3050 (2019). [PubMed: 30687308]
71. Tavernier SJ, Osorio F, Vandersarren L, Vetters J, Vanlangenakker N, Van Isterdael G, Vergote K, De Rycke R, Parthoens E, van de Laar L, Iwawaki T, Del Valle JR, Hu CC, Lambrecht BN, Janssens S, Regulated IRE1-dependent mRNA decay sets the threshold for dendritic cell survival. Nat. Cell Biol 19, 698–710 (2017). [PubMed: 28459443]
72. Goodall JC, Wu C, Zhang Y, McNeill L, Ellis L, Saudek V, Gaston JS, Endoplasmic reticulum stress-induced transcription factor, CHOP, is crucial for dendritic cell IL-23 expression. Proc. Natl. Acad. Sci. U.S.A 107, 17698–17703 (2010). [PubMed: 20876114]
73. Mogilenko DA, Haas JT, L'homme L, Fleury S, Quemener S, Levavasseur M, Becquart C, Wartelle J, Bogomolova A, Pineau L, Molendi-Coste O, Lancel S, Dehondt H, Gheeraert C, Melchior A, Dewas C, Nikitin A, Pic S, Rabhi N, Annicotte JS, Oyadomari S, Velasco-Hernandez T, Cammenga J, Foretz M, Viollet B, Vukovic M, Villacreces A, Kranc K, Carmeliet P, Marot G, Boulter A, Tavernier S, Berod L, Longhi MP, Paget C, Janssens S, Staumont-Sallé D, Aksoy E, Staels B, Dombrowicz D, Metabolic and innate immune cues merge into a specific inflammatory response via the UPR. Cell 177, 1201–1216.e19 (2019). [PubMed: 31031005]
74. Márquez S, Fernández JJ, Terán-Cabanillas E, Herrero C, Alonso S, Azogil A, Montero O, Iwawaki T, Cubillos-Ruiz JR, Fernández N, Crespo MS, Endoplasmic reticulum stress sensor IRE1α enhances IL-23 expression by human dendritic cells. Front. Immunol 8, 639 (2017). [PubMed: 28674530]
75. Niederreiter L, Fritz TM, Adolph TE, Krismer AM, Offner FA, Tschurtschenthaler M, Flak MB, Hosomi S, Tomczak MF, Kaneider NC, Sarcevic E, Kempster SL, Raine T, Esser D, Rosenstiel P, Kohno K, Iwawaki T, Tilg H, Blumberg RS, Kaser A, ER stress transcription factor Xbp1 suppresses intestinal tumorigenesis and directs intestinal stem cells. J. Exp. Med 210, 2041–2056 (2013). [PubMed: 24043762]
76. Kirkling ME, Cytlak U, Lau CM, Lewis KL, Resteu A, Khodadadi-Jamayran A, Siebel CW, Salmon H, Merad M, Tsirigos A, Collin M, Bigley V, Reizis B, Notch signaling facilitates in vitro generation of cross-presenting classical dendritic cells. Cell Rep. 23, 3658–3672.e6 (2018). [PubMed: 29925006]
77. Lee AH, Iwakoshi NN, Glimcher LH, XBP-1 regulates a subset of endoplasmic reticulum resident chaperone genes in the unfolded protein response. Mol. Cell. Biol 23, 7448–7459 (2003). [PubMed: 14559994]
78. Dobin A, Davis CA, Schlesinger F, Drenkow J, Zaleski C, Jha S, Batut P, Chaisson M, Gingeras TR, STAR: Ultrafast universal RNA-seq aligner. Bioinformatics 29, 15–21 (2013). [PubMed: 23104886]
79. Li B, Dewey CN, RSEM: Accurate transcript quantification from RNA-seq data with or without a reference genome. BMC Bioinformatics 12, 323 (2011). [PubMed: 21816040]
80. Love MI, Huber W, Anders S, Moderated estimation of fold change and dispersion for RNA-seq data with DESeq2. Genome Biol. 15, 550 (2014). [PubMed: 25516281]
81. Heinz S, Benner C, Spann N, Bertolino E, Lin YC, Laslo P, Cheng JX, Murre C, Singh H, Glass CK, Simple combinations of lineage-determining transcription factors prime cis-regulatory elements required for macrophage and B cell identities. Mol. Cell 38, 576–589 (2010). [PubMed: 20513432]

82. Wickham H, Francois R, Henry L, Muller K, dplyr: A Grammar of Data Manipulation (R package. version 0.8.0.1., 2019).
83. Wickham H, ggplot2: Elegant Graphics for Data Analysis (Springer-Verlag, 2016).
84. Wilke CO, cowplot: Streamlined Plot Theme and Plot Annotations for 'ggplot2' (R package. version 1.1.0, 2020).
85. Kolde R, pheatmap: Pretty Heatmaps (R package version 1.0.12, 2019).
86. Conway JR, Lex A, Gehlenborg N, UpSetR: An R package for the visualization of intersecting sets and their properties. Bioinformatics 33, 2938–2940 (2017). [PubMed: 28645171]
87. Nikolic T, Woittiez NJC, van der Slik A, Laban S, Joosten A, Gysemans C, Mathieu C, Zwaginga JJ, Koeleman B, Roep BO, Differential transcriptome of tolerogenic versus inflammatory dendritic cells points to modulated T1D genetic risk and enriched immune regulation. Genes Immun. 18, 176–183 (2017). [PubMed: 28794505]

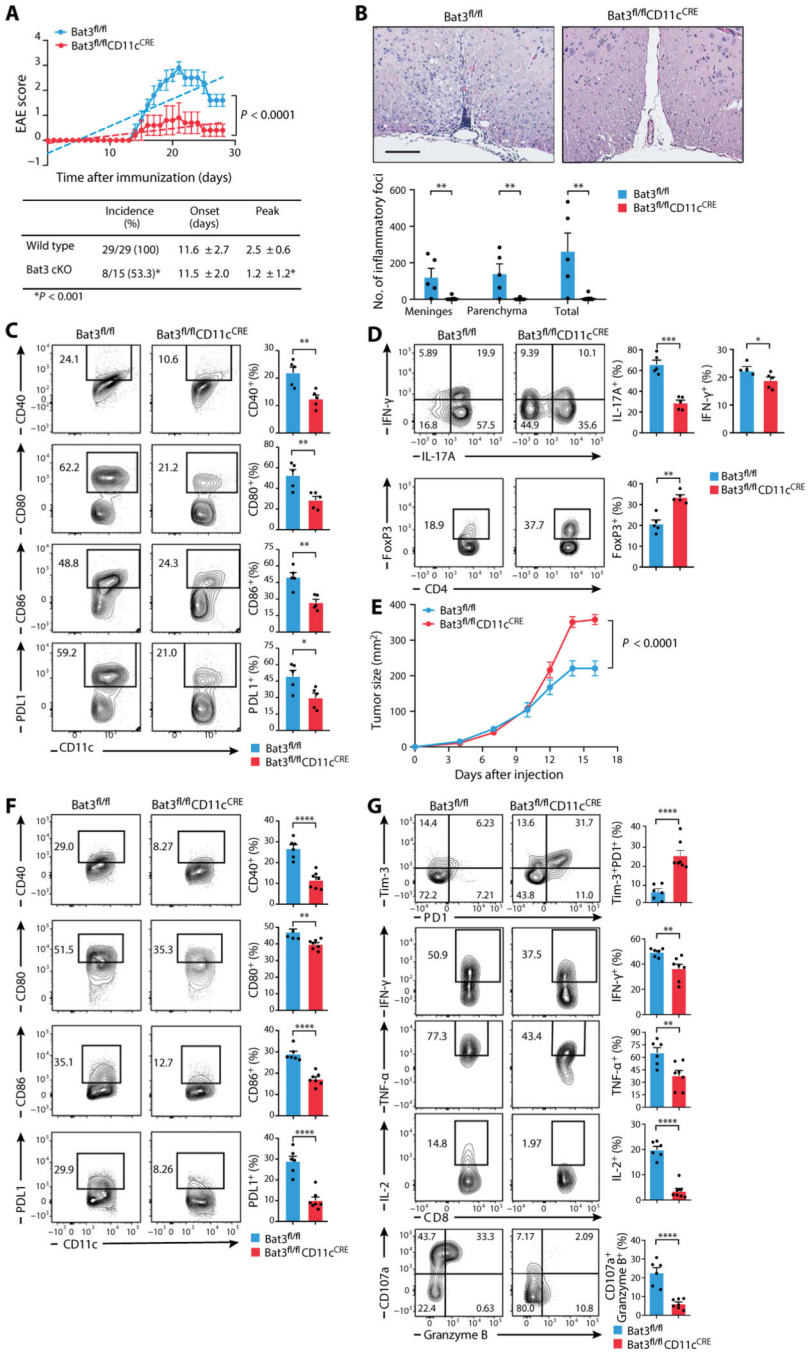

Fig. 1. The absence of expression of Bat3 in DCs pro-foundly affects DC–T cells cross-talk.

(**A**) Top: Summary plot of mean clinical scores of *Bat3*$^{fl/fl}$ and *Bat3*$^{fl/fl}$*CD11c*^{CRE} mice subjected to EAE induction by $MOG_{35–55}$ emulsions. Bottom: Summary table of EAE disease of littermate control *Bat3*$^{fl/fl}$ and *Bat3*$^{fl/fl}$*CD11c*^{CRE} mice (n = 15 to 29, linear mixed model). (**B**) Top: Representative hematoxylin and eosin–stained spinal cord section showing inflammatory foci in meninges and parenchyma of a representative Bat3$^{fl/fl}$ mouse. There is no inflammation in the Bat3$^{fl/fl}$CD11c^{CRE} mouse. Bottom: Graph demonstrates counts of inflammatory foci. Scale bar, 100 μm. Tissues collected from the same experiment from

(A). Unpaired multiple *t* test. (**C**) The activation status of cDCs ($CD3^{-}CD19^{-}NK1.1^{-}SiglecF^{-}Ly6^{-}F4/80^{-}CD45^{hi}CD11c^{hi}$ cells) infiltrating the spinal cord and brain of $Bat3^{fl/fl}$ and $Bat3^{fl/fl}CD11c^{CRE}$ mice on day 9 after immunization with $MOG_{35–55}$ emulsions ($n = 5$, unpaired Student's *t* test). (**D**) The frequency of IFN-γ^{+}, IL-$17A^{+}$, or $FoxP3^{+}$ $CD4^{+}$ T cells infiltrating the spinal cord and brain of $Bat3^{fl/fl}$ and $Bat3^{fl/fl}CD11c^{CRE}$ mice at the peak of EAE disease ($n = 5$, unpaired Student's CRE *t* test). (**E**) Tumor growth curve of MC38-OVA^{dim} cells implanted in $Bat3^{fl/fl}$ and $Bat3^{fl/fl}CD11c^{CRE}$ mice subcutaneously ($n = 6$ to 7, linear mixed model). Mean tumor growth is shown. (**F** and **G**) Infiltrating myeloid cells and TILs were harvested from mice bearing MC38-OVA^{dim} at a tumor size of 120 to 150 mm^2 as determined by the growth observed in WT control ($n = 6$, unpaired Student's *t* test). (F) Fluorescence- activated cell sorting (FACS) analysis of MHC-II, CD40, CD80, CD86, and PDL1 expression on cDCs. (G) FACS analysis of Tim-$3^{+}PD1^{+}$, TNF-α^{+}, IFN- γ^{+}, and $CD107a^{+}$Granzyme $B^{+}CD8^{+}$ TILs. Data are representative of at least three independent experiments with similar results. Error bars show means ± SEM. $*P < 0.05$, $**P < 0.01$, and $***P < 0.001$, and $****P < 0.0001$.

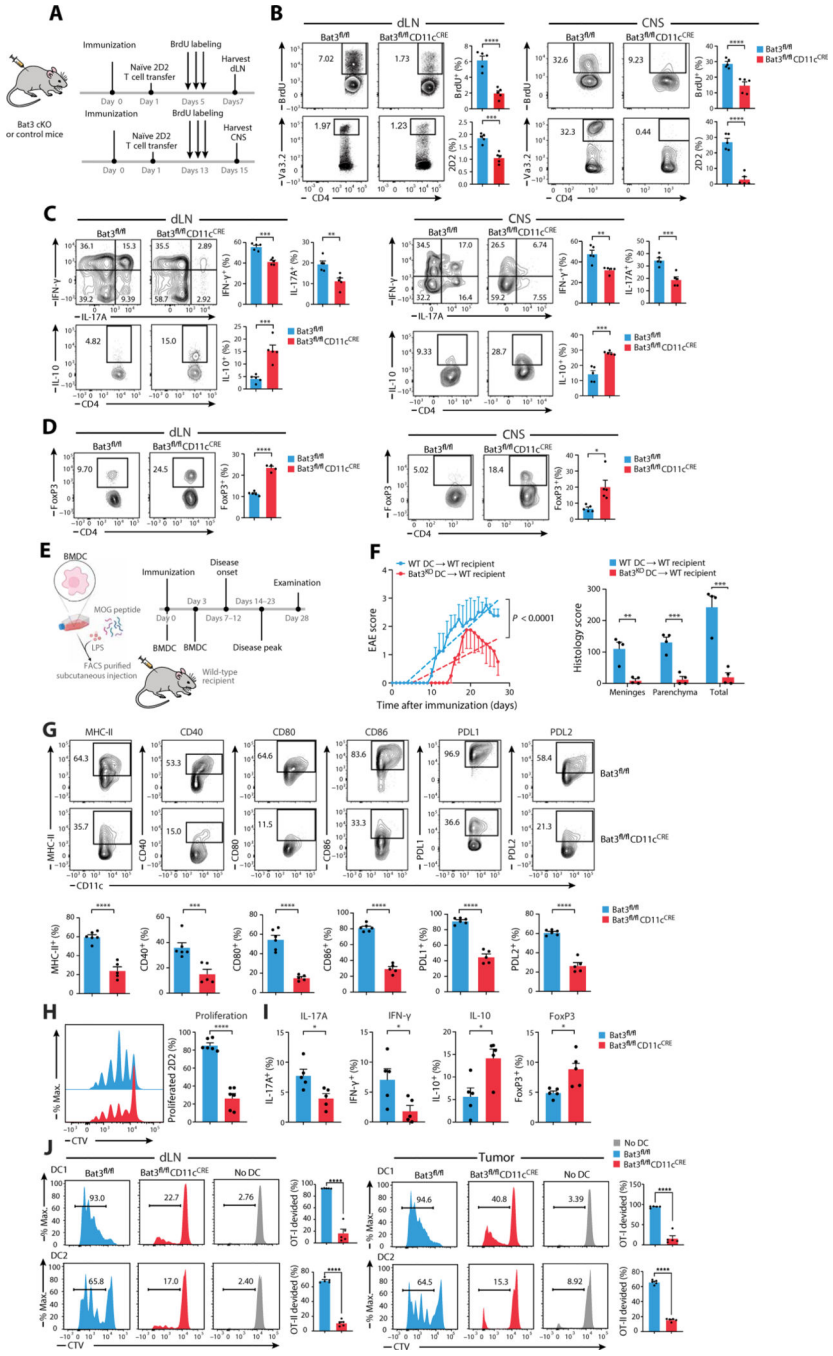

Fig. 2. Bat3 regulates the functional plasticity of DCs in vivo.

(**A**) Schematic illustration of experimental procedures used for 2D2 naïve T cells transfer to mice subjected to EAE induction by $MOG_{35–55}$ emulsions. (**B** to **D**) dLN and CNS infiltrating lymphocytes were obtained from the *Bat3*$^{fl/fl}$ and *Bat3*$^{fl/fl}$*CD11c*^{CRE} mice at the onset (day 7) or the peak of disease with an average score of 3 (day 15) after EAE induction ($n = 5$). (B) Frequency of BrdU$^+$ cells and 2D2 (Vα3.2$^+$ CD4$^+$ T) cells among the CD4$^+$ T cells in dLN (left) and CNS (right). (C) Frequency of IFN-γ$^+$, IL-17A$^+$, and IL-10$^+$ cells among the 2D2 cells in dLN (left) and CNS (right). (D) Frequency of FoxP3$^+$ cells among

the 2D2 cells in the dLN (left) and CNS (right). (**E**) Schematic illustration of BMDCs derived from *Bat3*$^{fl/fl}$ and *Bat3*$^{fl/fl}$*CD11c*^{CRE} mice transfer to WT recipient mice subjected to EAE induction by $MOG_{35–55}$ emulsions. (**F**) Left: Average clinical score of EAE in WT recipient mice. Right: The average histological score of CNS and spinal cord sections of the recipient mice ($n = 4$). (**G**) FACS analysis of the MHC-II$^+$, CD40$^+$, CD80$^+$, CD86$^+$, PDL1$^+$, and PDL2$^+$CD11c^{hi} cells from BMDCs derived from WT or *Bat3*$^{fl/fl}$*CD11c*^{CRE} mice activated by LPS (500 ng/ml) for 24 hours ($n = 5$ to 6). (**H** and **I**) BMDCs derived from WT or *Bat3*$^{fl/fl}$*CD11c*^{CRE} mice were cocultured with CellTrace Violet (CTV)–labeled 2D2 T cells for 72 hours. 2D2 cell proliferation and cytokine production were assessed by flow cytometry. (H) Frequency of proliferated 2D2 cells ($n = 6$). (I) Frequency of IFN-γ^+, IL-17A$^+$, IL-10$^+$, and FoxP3$^+$ cells gated on the proliferated 2D2 cells ($n = 5$). Data are representative of at least three independent experiments. Error bars show means ± SEM. (**J**) CellTrace Violet-dilution analysis of OT-I and OT-II cells co-cultured with OVA protein-pulsed tDCs isolated from tumor of dLN of *Bat3*$^{fl/fl}$ or *Bat3*$^{fl/fl}$*CD11c*^{CRE} mice bearing MC38-OVA^{dim} tumors for 2 weeks. *$P < 0.05$, **$P < 0.01$, ***$P < 0.001$, and ****$P < 0.0001$, unpaired Student's *t* test.

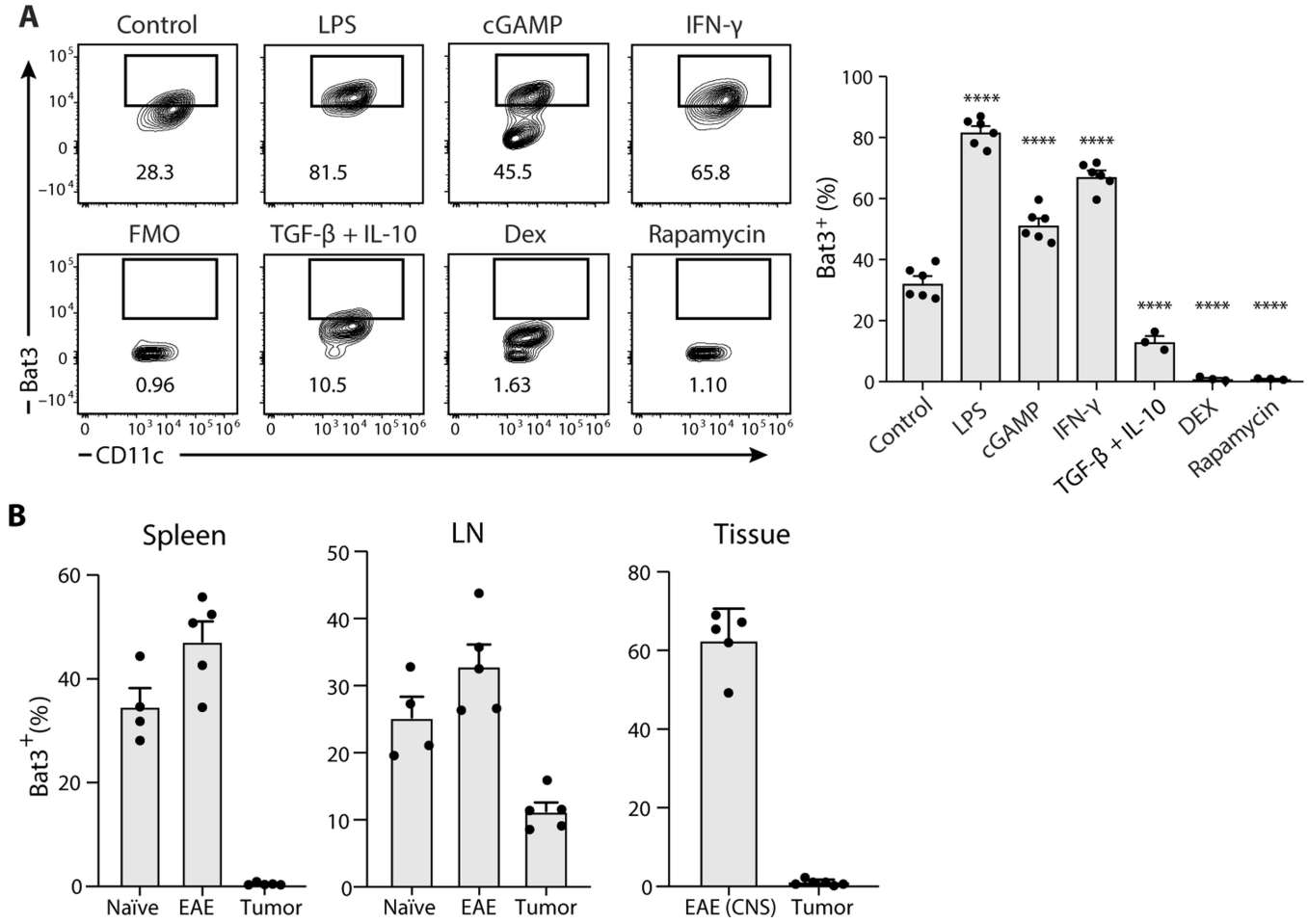

Fig. 3. The expression level of Bat3 is regulated by microenvironmental cues.

(**A**) Frequency of Bat3^{+}CD11c^{hi} BMDCs activated by the indicated TLR agonists (LPS), STING agonist [cyclic guanosine monophosphate–adenosine monophosphate (cGAMP)], and IFN-γ, and indicated tolerance inducing reagents (TGF-β/IL-10, DEX, and rapamycin) (one-way ANOVA). (**B**) Frequency of Bat3^{+} DCs in the spleen and iLN in mice in steady state, with EAE or tumor-bearing status. Frequency of Bat3^{+} DCs was also compared between DC infiltrating the CNS in EAE and tumor mass in MC38-OVA^{dim} cells implanted mice (one-way ANOVA, unpaired Student's *t* test). Data are representative of at least three independent experiments ($n = 3$ to 6). Data are shown as means ± SEM. ****$P < 0.0001$.

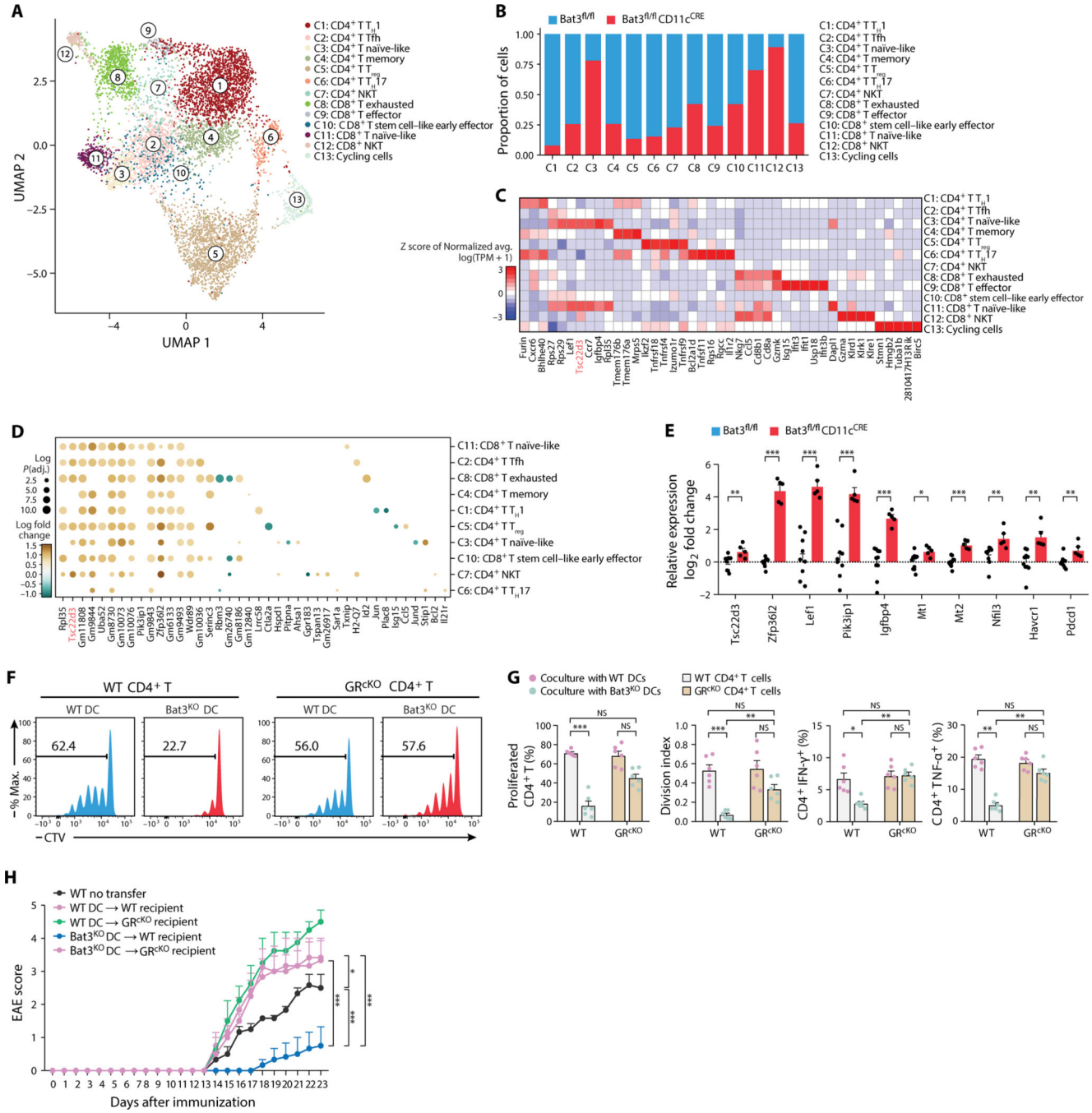

Fig. 4. The CNS T cell landscape is altered in the absence of Bat3 expression in DCs.

(**A**) UMAP visualization of CNS-infiltrating T cells isolated from the *Bat3*$^{fl/fl}$ and *Bat3*$^{fl/fl}$*CD11c*^{CRE} mice (n = 5 per genotype pooled) immunized with $MOG_{35–55}$ emulsion. Colors indicate unbiased T cell classification via graph-based clustering. Each dot represents an individual cell. Tfh, T follicular helper. (**B**) Bar plots representing proportion of CNS-infiltrating T cells from *Bat3*$^{fl/fl}$ and *Bat3*$^{fl/fl}$*CD11c*^{CRE} mice in the different clusters. (**C**) Heatmap reports scaled expression [log TPM (transcripts per million) values] of discriminative gene sets for each cluster defined in Fig. 6A. *Tsc22d3* was enriched in CNS-

infiltrating T cells from *Bat3*$^{fl/fl}$*CD11c*^{CRE} mice. (**D**) Dot plot of top DE genes (DEGs) of different clusters of CNS-infiltrating T cells from *Bat3*$^{fl/fl}$ and *Bat3*$^{fl/fl}$*CD11c*^{CRE} mice. Only the clusters that passed the $\log_2$ fold change of >1 ($P < 0.05$) are shown. (**E**) Expression of steroidogenesis genes in CD4$^+$ T cells in the iLN from the *Bat3*$^{fl/fl}$ or *Bat3*$^{fl/fl}$*CD11c*^{CRE} mice at day 8 after immunization with $MOG_{35–55}$ emulsion ($n = 5$ to 10, unpaired multiple *t* test). (**F** and **G**) BMDCs derived from *Bat3*$^{fl/fl}$ or *Bat3*$^{fl/fl}$*CD11c*^{CRE} mice were cocultured with CellTrace Violet–labeled naïve CD4$^+$ T cells from either Nr3c1$^{fl/fl}$ or Nr3c1$^{fl/fl}$dLck^{CRE} mice for 72 hours. T cell proliferation and cytokine production were assessed by flow cytometry. $n = 6$. (F) Frequency of proliferated T cells. (G) Frequency of proliferated T cells, division index, and IFN-γ^+ and TNF-α^+ cells among the proliferated cells (two-way ANOVA). (**H**) Clinical score of EAE in the $MOG_{35–55}$ emulsion immunized Nr3c1$^{fl/fl}$ or Nr3c1$^{fl/fl}$ dLck^{CRE} (GR^{cKO}) that received BMDCs derived from either *Bat3*$^{fl/fl}$ or *Bat3*$^{fl/fl}$*CD11c*^{CRE} mice ($n = 4$ to 6). Data are representative of three independent experiments. Error bars show means ± SEM. NS, not significant. *$P < 0.05$, **$P < 0.01$, and ***$P < 0.001$.

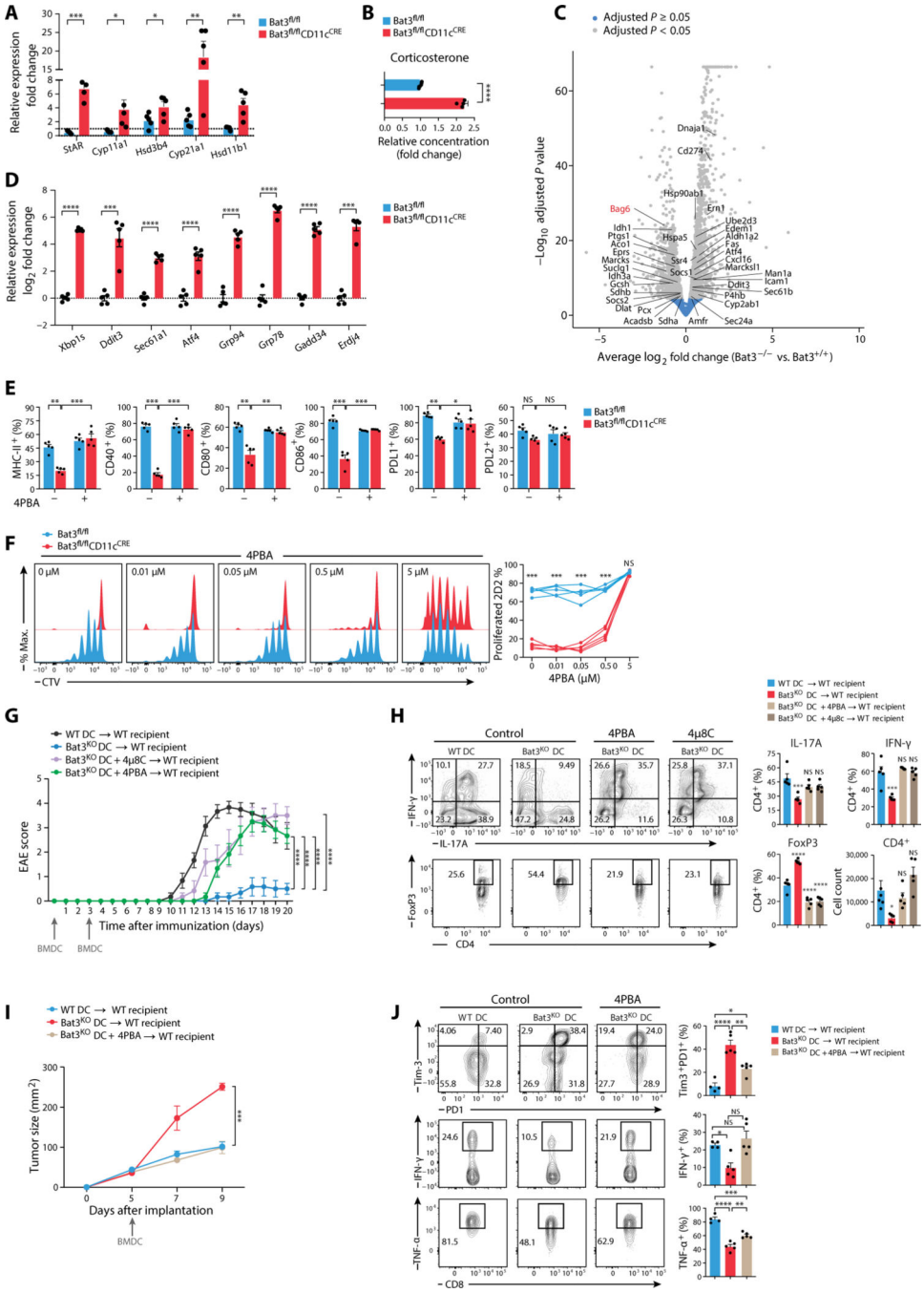

Fig. 5. Enhanced activation of UPR leads to acquisition of regulatory-like features by Bat3-deficient DCs.

(**A**) Expression of the gene encoding enzymes involved in glucocorticoid biosynthesis in BMDCs derived from the *Bat3*$^{fl/fl}$ or *Bat3*$^{fl/fl}$*CD11c*^{CRE} mice and treated with LPS (500 ng/ml) for 6hours (n=5) (unpaired multiple t test). (**B**) BMDCs were treated with LPS (500 ng/ml) for 96 hours, and the supernatant was collected. The corticosterone levels in the culture medium were quantified by ELISA (n = 5 per group, unpaired Student's t test). (**C**) Volcano plot showing the DEGs between BMDCs derived from *Bat3*$^{fl/fl}$ and

Bat3$^{fl/fl}$*CD11c*^{CRE} mice on LPS stimulation; plotted values are normalized gene expression units (transcripts per million) and scaled across samples in all conditions (n=5). (**D**) Expression of *Xbp1s*, *Sec61a1*, *Atf4*, *ERdj4*, *Ddit3*, *Grp94*, *Gadd34*, and *Grp78* in BMDCs derived from *Bat3*$^{fl/fl}$ and *Bat3*$^{fl/fl}$ *CD11c*^{CRE} mice treated with LPS (500 ng/ml) (n = 5). Data were normalized to endogenous actin levels in each sample (unpaired multiple *t* test). (**E** and **F**) LPS-stimulated BMDCs derived from *Bat3*$^{fl/fl}$ or *Bat3*$^{fl/fl}$*CD11c*^{CRE} mice were treated with 4PBA or vehicle control, respectively, for 8 hours (n=5). (E) Frequency of MHC-II^{+}, CD40^{+}, CD80^{+}, CD86^{+}, PDL1^{+}, and PDL2^{+} CD11c^{hi} BMDCs in the indicated groups (two-way ANOVA). (F) Proliferation of CellTrace Violet–labeled 2D2 cell cocultured with BMDCs treated with indicated dose of 4PBA for 72hours (unpaired multiple t test). (**G**) Clinical score of EAE in $MOG_{35–55}$ emulsion immunized WT mice that received indicated BMDCs subcutaneously at days 0 and 3 after immunization (n = 5 to 6, linear mixed model). (**H**) Frequency of total CD4^{+} T cells (among CD45^{hi}) and IFN-γ $^{+}$ cells (among CD45^{hi} CD4^{+}) infiltrating in the CNS (n=5 to 6, one-way ANOVA). (**I**) OVA protein–pulsed BMDCs derived from *Bat3*$^{fl/fl}$ or *Bat3*$^{fl/fl}$*CD11c*^{CRE} mice treated with 4PBA were administrated subcutaneously in WT mice implanted with MC38-OVA^{dim} tumors. Mean tumor growth is shown (n = 5, linear mixed model). (**J**) Frequency of IFN-γ + CD8^{+} TILs (n = 5, one-way ANOVA). Data are representative of three independent experiments. Error bars show means ± SEM. *P< 0.01, ***P < 0.001, and ****P < 0.0001.

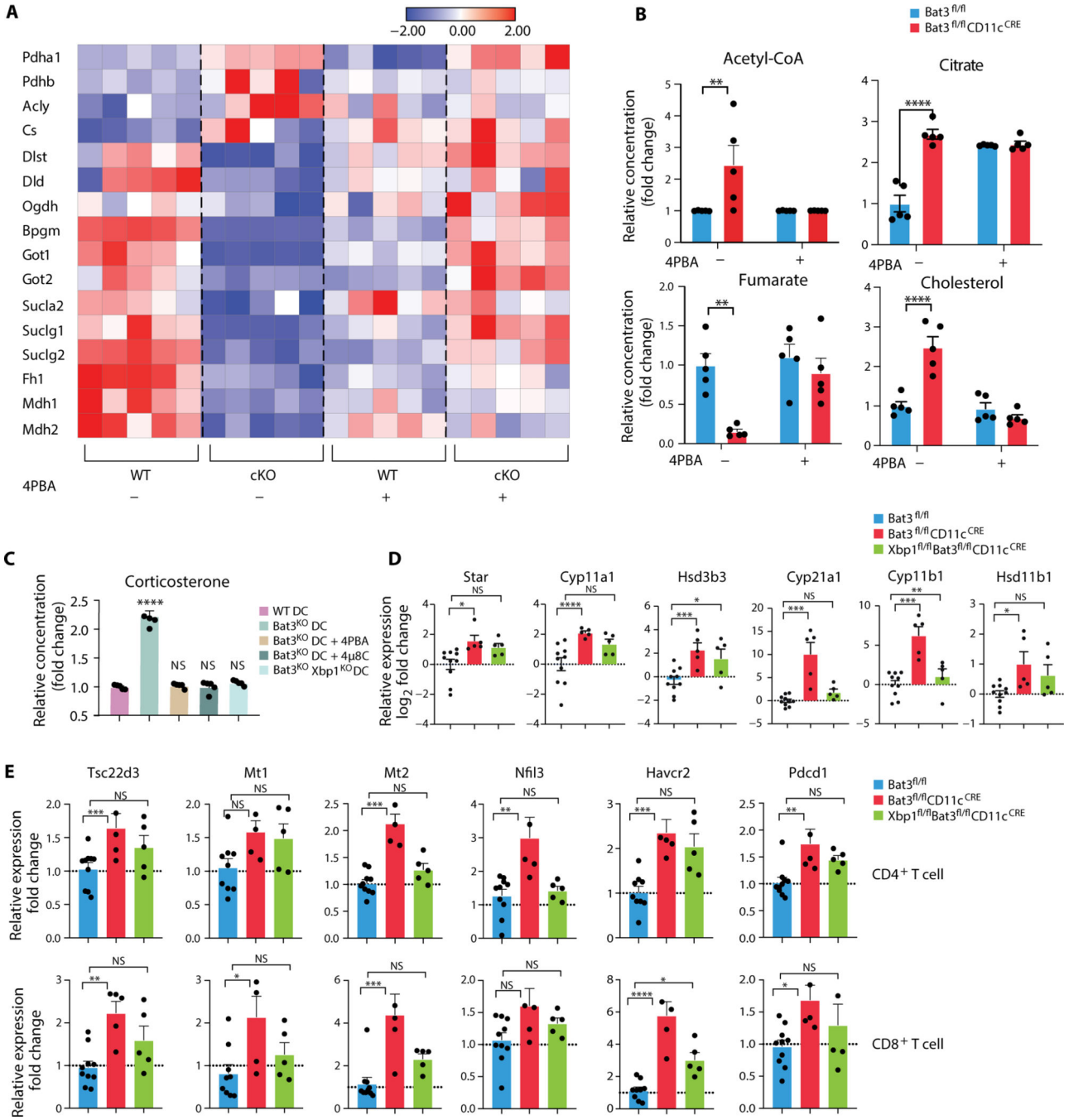

Fig. 6. Bat3-mediated ER stress regulates regulatory phenotype of DCs by calibrating cell-intrinsic steroidogenesis.

(**A**) Heatmap representation of BMDCs subjected to qPCR. Plotted values are *z* score of fold changes normalized to endogenous actin levels in each sample ($n = 5$). (**B**) Relative levels of acetyl-CoA, citrate, fumarate, and cholesterol in control and Bat3^{ko} DCs, represented as fold change of untreated controls ($n = 5$, two-way ANOVA). (**C**) ELISA in supernatants collected from BMDC treated with indicated conditions for 96 hours. The concentration of corticosterone in supernatant from WT BMDCs was scaled to 1.0 as

control, and relative corticosterone levels were quantified as fold change of control group ($n = 5$, one-way ANOVA). (**D** and **E**) Cells were sorted from the inguinal LN of the *Bat3*$^{fl/fl}$, *Bat3*$^{fl/fl}$*CD11c*^{CRE} mice, or the *Xbp1*$^{fl/fl}$*Bat3*$^{fl/fl}$*CD11c*^{CRE} mice on day 8 after immunization with $MOG_{35–55}$ emulsion ($n = 5$ to 10, one-way ANOVA). (D) Expression of the gene encoding enzymes involved in glucocorticoid biosynthesis in dLN-derived DCs. (E) Expression of the glucocorticoid-responsive genes in dLN-derived $CD4^+$ T cells and $CD8^+$ T cells. Data are representative of three independent experiments with similar results. Error bars show means ± SEM. *$P < 0.05$, **$P < 0.01$, ***$P < 0.001$, and ****$P < 0.0001$.

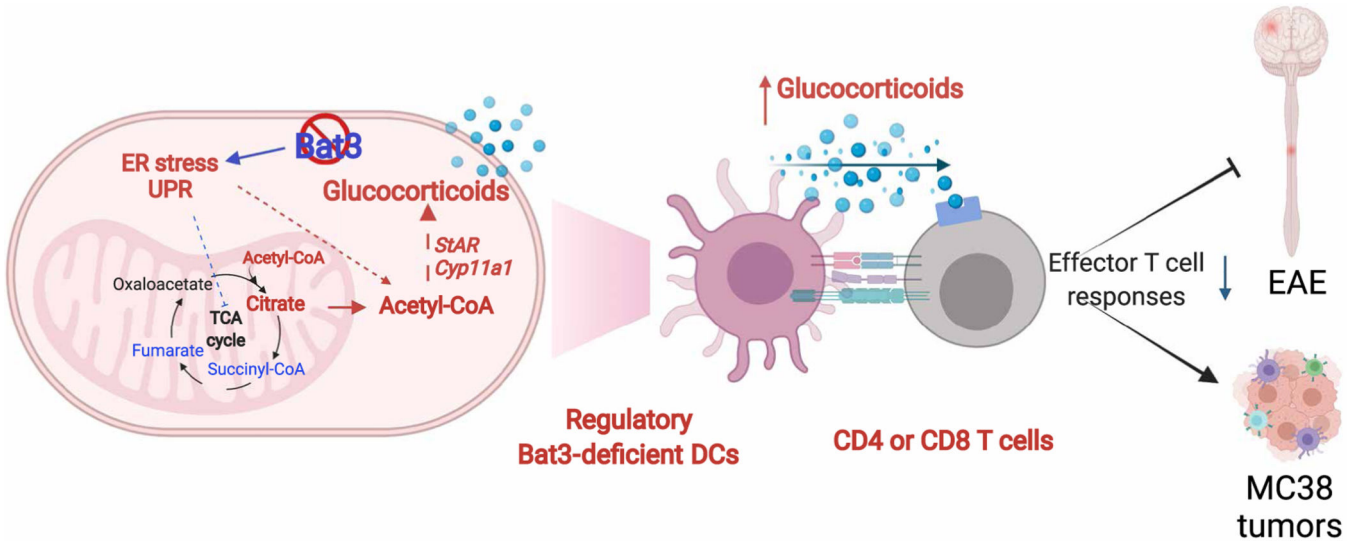

Fig. 7. Proposed model for Bat3 regulating the DC function.

Loss of Bat3 activates ER stress, which, in turn, inhibits the TCA cycle, leading to the accumulation of citrate. Citrate serves as a substrate for the synthesis of cholesterol that is broken down to produce glucocorticoids. DC-derived glucocorticoids act on T cells to inhibit autoreactive T cell responses in EAE and antitumor T cell responses in MC38 colon carcinoma.